An integrated model system to gain mechanistic insights into biofilm-associated antimicrobial resistance in *Pseudomonas aeruginosa* MPAO1

Adithi R. Varadarajan[1*,#], Raymond N. Allan[2,3,4*], Jules D. P. Valentin[5,6*], Olga E. Castañeda Ocampo[6], Vincent Somerville[1], Franziska Pietsch[7], Matthias T. Buhmann[5], Jonathan West[8,9], Paul J. Skipp[10], Henny C. van der Mei[6], Qun Ren[5], Frank Schreiber[7], Jeremy S. Webb[2,3], Christian H. Ahrens[1,#]

[1]Agroscope, Research Group Molecular Diagnostics, Genomics & Bioinformatics and SIB Swiss Institute of Bioinformatics, CH-8820 Wädenswil, Switzerland

[2]School of Biological Sciences and Institute for Life Sciences, University of Southampton, Southampton, SO17 1BJ, UK

[3]National Biofilms Innovation Centre, University of Southampton, Southampton, SO17 1BJ, UK

[4]School of Pharmacy, Faculty of Health and Life Sciences, De Montfort University, Leicester, LE1 9BH, UK.

[5]Laboratory for Biointerfaces, Empa, Swiss Federal Laboratories for Materials Science and Technology, St. Gallen, Switzerland.

[6]University of Groningen and University Medical Center Groningen, Department of BioMedical Engineering, Groningen, Netherlands.

[7]Federal Institute for Materials Research and Testing (BAM), Division of Biodeterioration and Reference Organisms, Berlin, Germany.

[8]Faculty of Medicine, University of Southampton, Southampton, SO17 1BJ, UK

[9]Centre for Hybrid Biodevices, University of Southampton, Southampton, SO17 1BJ, UK

[10]Centre for Proteomics Research, University of Southampton, Southampton, SO17 1BJ, UK

* shared first authorship
[#]Correspondence:
Dr. Christian Ahrens / Dr. Adithi Varadarajan
Agroscope & SIB Swiss Institute of Bioinformatics
Müller-Thurgau Strasse 29
CH-8820 Wädenswil, Switzerland
Phone: +41-58 460 6114
Fax: +41-58 460 6341
Email: [#]christian.ahrens@agroscope.admin.ch / [#]vadithi.ethz@gmail.com

Abstract

Pseudomonas aeruginosa MPAO1 is the parental strain of the widely utilized transposon mutant collection for this important clinical pathogen. Here, we validate a model system to identify genes involved in biofilm growth and biofilm-associated antibiotic resistance. Our model employs a genomics-driven workflow to assemble the complete MPAO1 genome, identify unique and conserved genes by comparative genomics with the PAO1 reference strain and genes missed within existing assemblies by proteogenomics. Among over 200 unique MPAO1 genes, we identified six general essential genes that were overlooked when mapping public Tn-seq datasets against PAO1, including an antitoxin. Genomic data were integrated with phenotypic data from an experimental workflow using a user-friendly, soft lithography-based microfluidic flow chamber for biofilm growth and a screen with the Tn-mutant library in microtiter plates. The screen identified hitherto unknown genes involved in biofilm growth and antibiotic resistance. Experiments conducted with the flow chamber across three laboratories delivered reproducible data on *P. aeruginosa* biofilms and validated the function of both known genes and genes identified in the Tn-mutant screens. Differential protein abundance data from planktonic cells versus biofilm confirmed upregulation of candidates known to affect biofilm formation, of structural and secreted proteins of type VI secretion systems and provided proteogenomic evidence for some missed MPAO1 genes. This integrated, broadly applicable model promises to improve the mechanistic understanding of biofilm formation, antimicrobial tolerance and resistance evolution in biofilms.

Keywords: *Pseudomonas aeruginosa,* biofilm formation, antibiotic resistance, *de novo* genome assembly, Tn-seq, essential genes, type VI secretion system, toxin-antitoxin systems, colistin

Introduction

Pseudomonas aeruginosa is a Gram-negative bacterium ubiquitously present in soil, water and different animal hosts [1]. As an opportunistic human pathogen [2] it can cause sepsis, and chronic wound and lung infections, especially in immunocompromised and cystic fibrosis patients. Two mechanisms complicate the treatment of *P. aeruginosa* infections. It forms recalcitrant biofilms in which the bacterial cells have an increased tolerance against antimicrobial compounds [3,4]. In addition, worldwide, multiple genetic variants have acquired antimicrobial resistance (AMR) traits [5], either through acquisition of resistance genes on mobile genetic elements such as plasmids [6] or through *de novo* mutations of chromosomal genes [7]. Furthermore, mutations affecting outer membrane porins and multi-drug efflux pumps can mediate resistance to almost all major antibiotic classes and several important biocides [8,9]. *P. aeruginosa* thus also belongs to the notorious group of ESKAPE pathogens, which represent the leading causes of worldwide nosocomial infections (*Enterococcus faecium*, *Staphylococcus aureus*, *Klebsiella pneumoniae*, *Acinetobacter baumannii*, *P. aeruginosa*, and *Enterobacter* species) [10,11]. Clinically most relevant are the resistances of *P. aeruginosa* strains against fluoroquinolones, aminoglycosides and beta-lactams, and against the last-resort antibiotic colistin (a polymyxin). In 2017, the World Health Organization (WHO) classified carbapenem-resistant *P. aeruginosa* strains in the highest priority group of “critical pathogens”. New treatment options informed by a more detailed molecular understanding of how and why resistance emerges during treatment, and how resistance is transmitted, are urgently needed for such critical pathogens.

Increased antimicrobial tolerance, a fundamental property of biofilms [12] is well-studied [13] and four mechanisms play a major role: (i) under nutrient-limited conditions in biofilms, *P. aeruginosa* expresses phenotypic variants, i.e., dormant cells that are less susceptible to antibiotics which target actively dividing cells [14]; (ii) *P. aeruginosa* form a protective extra-cellular matrix composed of polysaccharides, proteins and DNA that limits the diffusion of antimicrobial substances or sequesters them, such that biofilm cells experience a decreased

antimicrobial dosage [15]; (iii) anoxic conditions exist within the biofilm limiting the efficacy of antibiotics that require aerobic metabolic activity and the generation of reactive oxygen species [16]; (iv) sub-inhibitory concentrations of antibiotics induce increased rates of mutation, recombination and lateral gene transfer. The mutation rate in biofilms has been reported to be up to 100 times higher than in planktonic cells [17], significantly accelerating the development of antibiotic resistant mutants. Together, these mechanisms lead to hard-to-treat, chronic infections during which *P. aeruginosa* can persist and further evolve within the host in the presence of antimicrobial substances. Evolution within biofilms is highly parallel and differs significantly from evolution of planktonic cells [18]. However, the evolutionary drivers of within-biofilm AMR evolution remain poorly understood. Their study requires well-defined model systems and tools, including model strains with complete genomic background information, genetic tools and flow chambers allowing representative and reproducible growth of *P. aeruginosa* biofilms and deep sequencing data [18].

The canonical reference model strain for *P. aeruginosa* is PAO1, also referred to as PAO1-UW. Its complete genome sequence was published in 2000 [2], which allowed many breakthrough discoveries. However, a number of closely related PAO1 strains exist that differ in their phenotypic appearances [19]. These include *P. aeruginosa* strain MPAO1 [20], the parental strain of the widely utilized transposon insertion mutant library from the University of Washington (UW) [21]. Such mutant collections represent highly valuable resources to uncover new functions and condition-specific essential genes in genome-wide screens [21], for example genes relevant for resistance against certain antibiotics [22 23]. They have also been used to define so-called general essential genes, i.e., genes that were identified as essential under more than one relevant growth condition [24,25]. As a subset of the conserved core genes *of P. aeruginosa* PAO1 and PA14 were shown to exhibit differential essentiality [25], the approach to focus on those general essential genes that are furthermore conserved among key pathogen strains of a species is particularly promising [26]. However, the utility of such libraries to identify gain of function mutations is limited and polar effects need to be controlled for [27]. Notably, no

complete MPAO1 genome sequence was available. Improvements in next generation sequencing (NGS) technologies [28] and assembly algorithms nowadays allow researchers to readily generate complete *de novo* genome assemblies for most prokaryotes except a few percent of strains with highly complex repeat regions [29]. Such fully resolved genomes are advantageous compared to fragmented short read-based genome assemblies that can sometimes even miss conserved core genes [30]; they are an ideal basis for subsequent functional genomics and systems biology studies, and allow to identify so far missed genes in genome annotations by proteogenomics [31].

Here, we set out to develop, validate and make available a model system to study the biofilm-associated adaptation to antimicrobials and AMR evolution in *P. aeruginosa* MPAO1. Conceptually, the model was designed to integrate genotype information with phenotypic data and to leverage the valuable genetic tools and wealth of functional genomics datasets that exist for important bacterial model organisms. Important elements include the complete MPAO1 genome sequence and the design for a standardized flow chamber based on accessible soft lithography replication in poly(dimethylsiloxane) (PDMS) that can deliver laminar flow conditions relevant to typical biofilm niches. Comparative genomics with the PAO1-UW reference strain uncovered numerous MPAO1-unique genes. Strikingly, these included 39 essential genes that had been missed so far by performing reference-based mapping of public Tn-seq datasets. Proof of principle experiments highlighted reproducible biofilm growth using the microfluidic flow chamber and identified hitherto unknown genes important for biofilm growth and biofilm-associated AMR through microtiter plate screening of the mutant library. A differential (planktonic vs. biofilm) proteomic dataset uncovered genes known to play a role in biofilm formation. Finally, a publicly available, integrated proteogenomics search database enables identification of unannotated genes in MPAO1.

Results

De novo genome assembly of MPAO1

The availability of a complete genome sequence is an important pre-requisite to study the phenotypic adaptation and evolution of resistance to antimicrobials in biofilms. An analysis of over 9,300 completely sequenced, publicly available bacterial genomes [29] (see Methods) listed 106 *P. aeruginosa* strains overall, two of which were *P. aeruginosa* PAO1 strains, including the PAO1 type strain (Genbank AE004091), also called PAO1-UW [2]. In contrast, the only strain annotated as MPAO1, i.e. the founder strain of the transposon mutant library available from the UW [21], had been sequenced with Illumina short reads, assembled into 140 contigs [32] and deposited (http://www.pseudomonas.com/strain/show?id=659; Genbank ASM24743v2) in the Pseudomonas genome DB [33]. To provide an optimal basis for subsequent functional genomics and evolution studies for *P. aeruginosa* strain MPAO1, we thus first sequenced and *de novo* assembled its complete genome. Due to the genomic differences reported for MPAO1 and PAO1 [20] and the fact that many of the 106 completely sequenced *P. aeruginosa* strains have difficult to assemble genomes with long repeat pairs in excess of 10 kilobases (kb) (38/106), so-called class III genomes [29], we used third generation long reads from Pacific Biosciences' (PacBio) RSII platform. By relying on size-selected fragments (average length 9 kb; see Methods), a single bacterial chromosome could be assembled. Additional genome polishing steps with Illumina MiSeq data (300bp, PE reads) allowed the removal of remaining homopolymer errors in the PacBio assembly [34]. The final, high-quality MPAO1 genome consisted of one chromosome of 6,275,467 bp and coded for 5,926 genes (Genbank CP027857; **Table 1**). An overview of selected predicted genome features (see Methods) is shown in Supplementary **Table 1**. To facilitate data mining and comparison, we also provide an extensive annotation of all 5,799 protein-coding genes. This includes information on conserved and MPAO1-unique genes compared to PAO1, the respective reciprocal best BLAST hits, protein domains, families, Gene Ontology (GO) classification, predictions of subcellular localization, lipoproteins, secreted and described

membrane-localized proteins, as well as gene essentiality status and protein abundance data below (Supplementary **Data 1**).

Comparative genomics of MPAO1 and PAO1 strains

An alignment of our *de novo* assembled MPAO1 genome with that of the MPAO1/P1 strain [32] revealed that overall, 42,813 bp of our complete genome sequence were missed by the 140 contigs of the available fragmented Illumina assembly (**Fig. 1a**). This comprised 66 genes (52 protein coding genes, (CDS)) either missed completely or partially, including eight of 12 rRNA genes (75%) and six of 63 tRNA genes (11%). Among the CDS, the essential gene *ftsY* encoding the signal recognition particle-docking protein FtsY was missing, four of eight (50%) non-ribosomal peptide synthetase (NRPS) genes, three of six (50%) filamentous hemagglutinin N-terminal domain protein coding genes and three of 10 (30%) type VI secretion system (T6SS) VgrG effector proteins (Supplementary **Data 1**). The analysis of the number of interrupted genes or pseudogenes also confirmed the fragmented nature of the MPAO1/P1 genome compared to the complete genomes of both our assembly and the PAO1-UW type strain (Supplementary **Fig. 1**). Importantly, a key study of the genotypic and phenotypic diversity of *P. aeruginosa* PAO1 strains recently reported 10 PAO1/MPAO1 laboratory isolates as complete genomes [19]. As all 10 genomes have been assembled using Illumina data into sets of contigs, strictly speaking, they are not fully assembled, closed genome sequences. Indeed, the genomes of the two MPAO1 strains in that list (PAO1-2017-E, 71 contigs, whole genome shotgun (WGS) QZGA00000000 and PAO1-2017-I, 70 contigs, WGS QZGE00000000) also lacked a similar amount of genomic sequence (56.5 and 59.4 kb) and number of genes (55, 62) or CDS (40, 47) respectively, compared to our complete genome (Supplementary **Data 1**).

Next, to explore the extent of strain-specific genomic differences, we created an alignment of our *de novo* assembled MPAO1 genome with that of *P. aeruginosa* strain PAO1-UW. This analysis confirmed the major differences reported previously [20], i.e. the presence of a third

prophage region (12.8 kb, 20 genes; genome coordinates 5,241,813 - 5,254,613) in strain MPAO1 (**Fig. 1b**) and the absence of a ~1 kb genome fragment (leading to a pseudogene annotation for MPAO1_24940 in MPAO1). An analysis of smaller differences between the genomes confirmed the 16 SNPs reported previously [20], and identified 176 additional SNPs and INDELs between MPAO1 and PAO1 that had not been reported by Klockgether and colleagues [20] (Supplementary **Data 2**).

Notably, while the overall number of predicted genes was close for both strains (**Table 1**), we observed 232 gene clusters specific to strain MPAO1 and 21 clusters specific to strain PAO1-UW (**Fig. 1c**), suggestive of potentially relevant differences between the strains. The annotation of the shared (core) and strain-specific (unique) gene clusters is provided in Supplementary **Data 3**. This analysis indicated that a sizeable set of genes were specific to the MPAO1 genome, and that mapping datasets obtained from this strain back to the PAO1-UW genome could overlook important genes (see below). A gene ontology (GO) enrichment analysis of the MPAO1 unique proteins against all CDS in its genome revealed that the biological process “protein phosphorylation” was significantly enriched (p value < 0.01) with 10 hits among all genes including three among the unique genes (including a DNA helicase and 2 serine/threonine protein kinases; Supplementary **Table 2**). Furthermore, for the biological process “Bacteriocin immunity” five hits were found among all genes, two of which were among the unique MPAO1 genes (Supplementary **Table 2**).

Tn-seq data mapping

The complete MPAO1 genome sequence allowed us to re-analyze public Tn-seq datasets without the limitation of any remaining “genomic blind spots” that otherwise might preclude an identification of all essential genes [26], and the drawbacks of mapping Tn-seq data to a closely related reference genome. A re-mapping of MPAO1 Tn-seq datasets obtained from several conditions (LB medium, minimal medium, sputum and brain-heart infusion BHI medium) [24] against both the PAO1-UW genome and our MPAO1 genome (see Methods), confirmed our expectation. We indeed observed a higher percentage of mapped reads for

MPAO1 (roughly 0.1 - 0.35% of all mapped reads per sample; Supplementary **Table 3**) and unique insertion sites (roughly 0.2% more in MPAO1, Supplementary **Table 3**). Genes with no insertion or genes whose *p* value was less than 0.001 were considered essential (see Methods). Overall, 577 genes were classified as condition-specific essential in one of the three primary growth conditions LB medium, minimal medium, sputum (Supplementary **Data 4**), and 312 genes represented general essential genes, i.e., were essential in all three growth conditions, respectively (Supplementary **Fig. 2**). Importantly, close to 40 MPAO-1 unique genes were linked here with an essentiality status, as they were essential in one or more of the 16 Tn-seq libraries (Supplementary **Data 4**). By mapping data against the PAO1-UW genome, these genes had been previously overlooked in the analysis of essential *P. aeruginosa* genes.

Among these MPAO1-unique genes, we identified 18 genes that were essential in 50% or more of the Tn-seq runs, six of which represented general essential genes (**Table 2**). The general essential genes included two genes located in the prophage2 region, i.e., MPAO1_22380, a type II Phd/YefM family antitoxin gene located next to MPAO1_22375, coding for a RelE/ParE type toxin, and MPAO1_22450, a DNA-binding protein (**Fig. 2a**; arrows framed in red). A further general essential gene was MPAO1_00215 encoding for a hypothetical protein. MPAO1_00215 is located in a genomic region that harbors another essential gene (MPAO1_00230, Supplementary **Data 1**), that may represent an operon. Furthermore, the prophage 3 region unique to strain MPAO1, harbored a gene encoding a hypothetical protein (MPAO1_24865; **Fig. 2b**) that was essential in eight of 16 samples (Table 2). Conversely, MPAO1_24885 (addiction module antidote protein from the HigA family toxin-antitoxin (TA) system) from this region was classified as general essential (**Table 2**; 14 of 16 samples). Due to its homology to PA4674 in PAO1-UW, which is listed among the 352 general essential genes reported by Lee and colleagues and encodes the HigA antitoxin [24], it is not unique to MPAO1 (**Fig. 2b**). Together with the non-essential MPAO1_24890 (plasmid maintenance system killer protein; most similar to RelE-like toxins of the type II TA system HigB), MPAO1_24885 encodes for a TA system. However, there is no homolog

annotated for MPAO1_24890 in PAO1-UW. Therefore, due to this missing gene, the TA system was not identified in PAO1-UW. This finding again underlines the importance of having the actual and complete genome sequence to map functional data.

Reproducible formation of MPAO1 biofilms

The second important objective of our integrated model system was to enable the reliable generation of phenotypic data under conditions relevant for biofilm-growth. For this purpose, we focused on the development of a microfluidic flow chamber for reproducible biofilm formation that would allow us to subsequently identify genes relevant for biofilm growth and biofilm-associated AMR. The flow chamber was designed in such a way that we could assess the effects of hydrodynamic conditions [35], such as shear stress and controlled flow conditions. Our flow chamber was replicated in PDMS, a simple to use, transparent and breathable elastomer material that naturally adheres to glass. A straight microfluidic channel design was used (30 mm length x 2 mm width x 0.200 mm depth) (**Fig. 3a**, see Methods for further details). PDMS was selected due to its broad application in indwelling devices and implant materials [36]. The inlet and outlet of the microfluidic flow chamber comprised of sterile polytetrafluoroethylene (PTFE) tubing, a material that was chosen because it generally exhibits low bacterial adhesion. A syringe pump was used to deliver 5 µL/min ($\bar{u}$≈208 µm/s) flow inside the chamber to provide laminar flow conditions for bacterial adhesion and biofilm growth (the calculated Reynolds Number corrected for transport of water at 37 °C was 0.103; for details see Supplementary **Table 4**).

The reproducibility of a 72 h mature MPAO1 biofilm on the PDMS surface of the device was investigated by confocal laser scanning microscopy (CLSM) combined with live/dead staining using the dyes Syto9 and propidium iodide in three separate consortium laboratories all using the same microfluidic chamber mold (design publicly available; see Data Access) **(Fig. 3b, c)**. The biofilms formed in the three laboratories were consistent with data falling within 95% confidence intervals, the only difference being the observation of a reduced dead biovolume in one laboratory's model (Lab A; p value < 0.05). Biofilm formation was relatively

uniform throughout the flow channel with an average thickness of 16 µm and a small reduction observed towards the center of the channel (Inlet - 18.8 µm, 25% - 15.8 µm, 50% - 13.3 µm, 75% - 14.9 µm, Outlet - 17.3 µm). An average biovolume of 12.5 $\mu m^3/\mu m^2$ and dead biovolume of 8.4 $\mu m^3/\mu m^2$ was observed, again reducing towards the center of the device commensurate with the average biomass.

Screening experiments identify known and new genes relevant for biofilm formation and antibiotic resistance

The MPAO1 transposon mutant library was tested with a 96-well plate screening system that was devised to enable the identification of genes that affect biofilm formation and/or play a role in the development of biofilm-associated AMR (see Supplementary **Fig. 3**). A batch of 95 selected mutants (see Supplementary **Table 5)** was taken from the library to test the reliability of our protocol and to identify genes related to biofilm formation (in duplicate). Strain PW8965 harboring an insertion in *cbrB* (PAO1 identifier PA4726, MPAO1_25185), a transcriptional activator that forms part of the CbrA/CbrB two-component system important in catabolite repression [37], was found to produce the least amount of biofilm (**Fig. 4a**). In contrast, strain PW9283 mutated in *pntAA* (PA0195; MPAO1_01040), a NADPH/NAD^+ redox balance transhydrogenase [38], exhibited the highest biofilm biomass.

In a second step, selected mutants identified by the screening and the proteomic analysis (see below) were compared to positive and negative controls for biofilm formation (**Fig. 5a**). The *pslB mutant* (PA2232; MPAO1_14370), a gene whose product is involved in the synthesis and export of polysaccharides, was used as a reference point for low biofilm formation [39], while a *retS* mutant (PA4856; MPAO1_25880), encoding a pleiotropic regulator of multiple virulence factors, was used as reference point for high biofilm formation [40]. Overall, MPAO1 WT produced roughly twice the biofilm biomass of transposon mutants, suggesting that the transposon has an influence on biofilm formation and that it is more reliable to compare transposon mutants amongst each other. The transposon mutant PW7021 (an *arnB* mutant; PA3552; MPAO1_07345, see below) was chosen as an internal reference for biofilm formation as its biomass was found approximately midway through the

24h biofilm readings in **Fig. 4a**. We confirmed that the *cbrB* mutant produced significantly less biofilm biomass (*p* value < 0.001) than the *arnB* mutant, similar to the low biofilm forming *pslB* mutant. Biofilm growth of the *cbrB* mutant was also performed within the flow chamber to confirm the capacity of the device to assess differential biofilm formation. Similar to the 96-well plate screening assay, the *cbrB* mutant produced substantially less biofilm compared to the MPAO1 WT over 18 h in the flow chamber **(Fig. 5c)** and displayed a delayed exponential growth compared to WT and the other mutants tested (Supplementary **Fig. 4**). We also confirmed that the *pntAA* mutant produced higher biofilm biomass than other transposon mutants, similar to the high biofilm former *retS* mutant **(Fig. 5a)**. However, compared to the WT, the *retS* mutant produced comparable biofilm biomass, which is likely caused by a decrease of strain fitness due to the transposon insertion. An alternative explanation is that the effect of RetS cannot be measured after 24 h because it has been shown previously that RetS turns non-functional in *P. aeruginosa* WT after 8h following initial attachment [41]. Genes identified by the proteomic analysis (*vgrG1b*, *cdrA*, *aprX*; see result section below) did not seem to affect the biofilm formation of MPAO1 in the conditions tested.

Next, we tested the strains for their biofilm resistance to colistin and included the *arnB* mutant strain PW7021 as a positive control (see Supplementary **Fig. 3**). ArnB is a well-studied protein known to modify lipopolysaccharide (LPS) and play a key role in the resistance to colistin [42,43]. The recovery of biofilm cells after treatment with 25 µg/mL colistin was compared to the recovery of non-treated biofilm cells (**Fig. 4b**) (see Methods), as described previously [13]. This concentration of colistin was much higher than the minimal inhibitory concentration (MIC) used for the planktonic *P. aeruginosa* MPAO1 (8 µg/mL) allowing us to focus specifically on biofilm cells. As expected, the *arnB* mutant exhibited a very low recovery after colistin treatment (97% less than the control without colistin) (**Fig. 4b**). In contrast, the *arnB* mutant produced robust biofilms in the biofilm screening assay (**Fig. 4a**), a phenotype that was confirmed using the microfluidic chamber (**Fig. 4c**). Notably, the *cbrB* mutant strain grown as a biofilm was also found to be sensitive to colistin (90% less recovery than the control without colistin; **Fig. 4a**), which might be related with the low

amount of biofilm produced by this mutant. In contrast, the high biofilm former *pntAA* mutant exhibited high resistance towards colistin with a recovery close to the non-treated biofilm. In a second step, the resistance profile of the identified mutants was characterized in more detail by measuring the MIC of planktonic cells and the minimal biofilm inhibitory concentration (MBIC) towards colistin (**Fig. 5b**). Two independent experiments (with four replicates in total) confirmed the significantly higher sensitivity of planktonic cells of *arnB* and *cbrB* mutants compared to the WT (**Fig. 5b**). Additionally, inactivation of the genes *arnB* and *cbrB* reduced the biofilm recovery by 50% when 6 and 12 times less colistin was used, respectively, compared to the WT. Inactivating *cbrB* made MPAO1 biofilms more sensitive to low concentrations of colistin, but high concentrations seemed necessary to reach complete eradication (**Fig. 5b**). In contrast, inactivating *pntAA* increased *P. aeruginosa* resistance towards colistin both as planktonic and biofilm cells. Characterization of the genes identified in the proteomic study (see below) revealed that inactivating *cdrA* had no impact on MPAO1 resistance, but inactivation of *vgrG1b* [44] and *aprX* [45] increased MPAO1 resistance towards colistin both for planktonic and biofilm cells (**Fig. 5b**).

Protein abundance profiling of MPAO1 grown planktonically and in biofilms

To assess if we could identify proteins known to play a role in biofilm formation with the microfluidic chamber, we next generated shotgun proteomics data for MPAO1 cells grown to mid-exponential planktonic phase or as 72 h biofilms (3 replicates each). 1,530 and 1,728 proteins were identified in planktonic cells and biofilm, respectively, resulting in a combined 1,922 of the 5,799 annotated proteins (33.1%). Among the most significantly differentially abundant proteins ($\log_2$ fold change (FC) of ≥ 1 or ≤ -1 and adjusted p value ≤ 0.05; see Methods and Supplementary **Fig. 5**) several candidates were identified that have previously been linked with a role in biofilm formation. These included MuiA (MPAO1_18330) [46], CbpD (MPAO1_21730) [47], AcnA (MPAO1_17965) [48] and PilY1 (MPAO1_24155) [49] (**Fig. 5a, Table 3**; see Discussion). In addition, MPAO1_19625 was highly upregulated in biofilms (**Fig. 5a**). Notably, its PAO1 homolog AprX was reported to be secreted by a type I secretion system [45],

indicating that hypothetical proteins or proteins of unknown function can be linked to roles in biofilm formation and growth. We next looked for protein expression evidence for CDS missed in the fragmented short read genome assemblies. We found that 21 of the 52 CDSs missed in the MPAO1/P1 assembly were detected at the protein level (Supplementary **Data 1**). Notably, this included two proteins significantly upregulated in the biofilm, namely MPAO1_00520 (T6SS tip protein VgrG1b) located close to the H1-T6SS cluster [44] and MPAO1_24535 (**Fig. 5a**), the homolog of PAO1 CdrA, a cylic-di-GMP-regulated adhesin known to reinforce the biofilm matrix [50], again underlining the importance of a complete genome sequence for downstream functional genomics analyses. Notably, nine of 14 structural genes of H1-T6SS, one of overall three T6SSs in *P. aeruginosa* that helps it to prevail under stressful conditions [51], were upregulated around two-fold or more in biofilm (Supplementary **Fig. 6**). Similarly, all three VgrG1 proteins (1a-1c) that are co-regulated with the H1-TS66 [52] were upregulated in biofilm, while none of the other seven VgrG family members were expressed. Among the proteins down-regulated in 72h biofilms, three are associated with iron acquisition; isochorismate synthase (MPAO1_03800), a rate-limiting enzyme involved in the production of salicylate (precursor of the siderophore pyochelin) [53], the siderophore receptor MPAO1_23930 (PuiA), and the siderophore-interacting protein MPAO1_15475. Iron acquisition is deemed necessary for *P. aeruginosa* biofilm formation [54] so their down-regulation was unexpected, however, this response is likely circumvented by the utilization of alternative iron acquisition strategies including the high-affinity siderophore pyoverdine.

Finally, to identify unannotated short ORFs that may carry out important functions or new start sites, we created an integrated proteogenomics search database (iPtgxDB) for strain MPAO1 and PAO1 (Supplementary **Table 6**), which covers its entire coding potential [31]. A search combined with stringent result filtering (see Methods) allowed us to identify unambiguous peptide evidence [55] for a 44 aa longer proteoform of MPAO1_08365 (predicted by Prodigal, an *ab initio* gene prediction algorithm; **Fig. 5b**). In addition, we obtained proteogenomic evidence supporting a single nucleotide insertion in MPAO1_25975 in strain

MPAO1 as compared to PA4875 (annotated as pseudogene) in strain PAO1 (**Fig. 5c**). The peptide that supported this single nucleotide change at the amino acid level was identified with seven peptide spectrum matches (PSMs), illustrating the ability to identify SNP changes at the protein level, with implications for clinical proteomics.

Discussion

P. aeruginosa is a member of the ESKAPE pathogens, the lead cause of worldwide nosocomial infections [10]. Along with many other clinically relevant bacteria, it can form biofilms whose emergent properties [56] include a much higher tolerance to antimicrobials. Together with the increased mutation rates in biofilm compared to planktonic cells [17], this further complicates treatment and cure of biofilm-based infections [12,13]. The development of model systems allowing the study of antimicrobial tolerance mechanisms and the evolutionary dynamics that lead to AMR development in biofilms is thus of utmost priority. We here develop and validate such a model system for *P. aeruginosa* MPAO1 (**Fig. 6**). Conceptually, the model was designed to integrate genotype data with phenotypic information and to leverage the wealth of existing public genetic resources and functional genomics datasets. A complete, fully resolved genome sequence is one critical element [31,57], which recently allowed linking of genotypic differences of nine Pseudomonas plant microbiome isolates with their varying biocontrol potential [58]. While a complete genome existed for *P. aeruginosa* PAO1 [2], only three fragmented Illumina-based genome assemblies were available for MPAO1, the parental strain of the popular UW transposon mutant library [21]. These included strains MPAO1/P1 [32] and the recently sequenced PAO1-2017-E and PAO1-2017-I [19]. On average, they lacked between 55 to 66 genes (40 to 52 CDS) compared to our complete MPAO1 genome (Supplementary **Data 1**). For MPAO1/P1, these included the essential *ftsY*, an adhesin, several T6SS effectors (see below), and four of the overall eight NRPSs. NRPSs are highly relevant for AMR as they often represent enzymes involved in the biosynthesis of antibiotics [59]. In fact, due to the multi-resistant phenotype of ESKAPE

pathogens, concerted efforts aim to describe their NRPS gene clusters in search for new therapeutic approaches [60], reinforcing the need for complete genome sequences. Comparative genomics with the PAO1 type strain uncovered an inventory of conserved and strain-specific genes, and a list of genome-wide SNPs, extending an earlier study that had compared a subset of genomic regions [20]. Among the 232 MPAO1-unique gene clusters, bacteriocins [61] were enriched, which play a role in restricting the growth of closely related microbial competitors to gain an advantage in colonizing a variety of environments [62]. The complete MPAO1 genome enabled us to remap valuable existing Tn-seq datasets from relevant conditions [24], thereby identifying 39 MPAO1-unique essential genes that had escaped detection so far due to reference-based PAO1 mapping. 18 of these genes were essential in at least 50% of the 16 Tn-seq samples, and six represented general essential genes, including a Phd/YefM family type antitoxin (MPAO1_22380), which was essential in all samples. This is worth noting given the relevance of toxin-antitoxin systems for bacterial growth arrest and persistence [63]. Importantly, our data do not conflict with results from previous studies; rather, they open the field to study the roles of additional MPAO1-unique essential genes. Furthermore, our results suggest that groups planning to construct inventories of core essential genes in other pathogens, following the elegant approach of Poulsen et al. who had considered both relevant media mimicking different infection types and nine strains from different lineages of a *P. aeruginosa* phylogenetic tree [26], should ideally select complete genomes without any genomic blind spots.

To leverage the experimental arm of our model (**Fig. 6**), the consortium developed a PDMS microfluidic flow chamber for biofilm growth, which offers several significant advantages. It provides laminar flow conditions inside the channels (Supplementary **Table 4**), allows gas exchange, decreases the amount of growth medium, facilitates heat transfer, is inexpensive to replicate and permits imaging of the biofilm and easy harvesting for biochemical characterization. While the flow chamber can be used to monitor biofilm formation on both glass (oxygen impermeable) and PDMS, it is more relevant to investigate biofilm formation

on PDMS as a widely applied biomaterial used in indwelling devices and implants [36]. We observed that biofilms on PDMS formed a more homogeneous layer (**Fig. 3b**) as compared to the commonly observed mushroom-like structures of *P. aeruginosa* biofilms on glass [64]. This effect is not related to hydrodynamics as a flow chamber that previously has been shown to produce mushroom-like structures [65] has hydrodynamics ($\bar{u}\approx208$ µm/s and Re=0.24) comparable to our microfluidic chip. We speculate that the effect is most likely explained by two differences: (i) PDMS is oxygen permeable and can transport oxygen to the base of the biofilm that then manifest in overall biofilm structure, or (ii) slight differences in media composition.

The microfluidic data from the inter-laboratory trial on strain MPAO1 validated the utility of the flow chamber and allowed us to compare the phenotypes of WT and mutant strains of the UW transposon library. Important genes were identified with a microtiter plate screening assay and subsequently validated with the flow chamber. Proof of principle experiments confirmed the role of *arnB* (PA3552), i.e., a gene relevant for colistin resistance [42,43], both in biofilms grown in the 96-well plate screen and the flow chamber. In addition, a mutant lacking *cbrB* (PA4726) showed reduced resistance to colistin in biofilm and planktonic cells and formed very low amounts of biofilm in both the microtiter plate and flow chamber. In addition, inactivating *cbrB* was found to be as inhibitory for biofilm formation as inactivating the gene *pslB*, known to negatively influence biofilm matrix synthesis [39]. As part of the two-component system CbrAB, a mutation in the response regulator *cbrB* is known to negatively affect the use of several carbon and nitrogen sources [37]. Such a defect could explain the low growth rate, the low biofilm biomass and therefore the low resistance to colistin of this mutant. Using *P. aeruginosa* PA14, it was shown that a mutation in CbrA improved biofilm formation, while a mutation in CbrB did not [66]. However, these differences might be explained by strains (MPAO1 versus PA14) or growth media used (M9 versus BM2-biofilm medium). In contrast, our screening revealed that inactivating the transhydrogenase *pntAA* induced high biofilm formation, comparable to the known gene *retS*. While redox balance is known to correlate with biofilm morphology [67], the precise role of *pntAA* remains to be investigated. Together,

the combined data of the screen and flow chamber experiments demonstrated that genes previously not implicated in AMR and biofilm formation can be identified and that the function of known genes can be validated.

The differential proteomics data confirmed proteins known to play a role in biofilm formation and growth. These included MuiA, which inhibited swarming motility and enhanced biofilm formation (roles, that were validated in knockout strains) [46], and CbpD, for which higher protein abundance had been observed in late phases of biofilm growth; accordingly, mutants displayed a lower amount of biofilm growth and exopolysaccharides (EPS) [47]. Similarly, for two other proteins with significantly higher abundance in biofilms, inactivation studies showed that the gene encoding AcnA impaired biofilm formation and was required for microcolony formation [48], while increased abundance of PilY1 repressed swarming and increased biofilm formation, as confirmed by knockout experiments [49]. Biofilm exclusive protein expression was observed for MPAO1_00520, the T6SS VgrG1b effector protein [52], while the adhesin CdrA (MPAO1_24535) [50] was highly upregulated in biofilms. Both genes were missed in the MPAO1/P1 genome. CdrA forms a two-partner secretion system with CdrB, and both were upregulated under elevated c-di-GMP levels [50], in line with the upregulation we observed in biofilm. Moreover, an NRPS (MPAO1_14010) and the hypothetical protein MPAO1_19625 were significantly upregulated in biofilm (**Table 3**). The data provided insights beyond the top differentially abundant proteins. Notable examples included immunity protein TplEi [68] (PA1509, MPAO1_18250), a bacteriocin of the H2-T6SS [51], which was exclusively expressed in biofilm (Supplementary **Data 1**), and upregulation of nine of 14 structural members of H1-T6SS [51] (Supplementary **Fig. 6**). Active T6SSs have been associated with chronic infections in cystic fibrosis patients [52], and H1-T6SS plays an important role in dominance of *P. aeruginosa* in multi-species biofilms [69]. More sensitive and comprehensive proteomics studies are needed to overcome the limitation that only a third of the theoretical proteome was identified with our shotgun proteomics approach, e.g. by combining data dependent and data independent acquisition and the use of spectral libraries [70], allowing a more

comprehensive identification of lower abundant and small proteins, or by analyzing additional conditions or mutant strains under which tightly regulated proteins such as the Tse toxins (secreted substrates of the H1-T6SS) are expressed (Supplementary **Fig. S6**) [71].

The public MPAO1 (and PAO1) iPtgxDBs allow to identify missed genes by proteogenomics [31], which often encode short proteins (sProteins) that can carry out important functions [72,73]. Interestingly, Tn-seq data from the Manoil group had implied an essential genomic region in the PF1 phage region of PAO1-UW [24]. Re-mapping their data, we identified a general essential gene (MPAO1_22380) annotated in our MPAO1 genome whose homolog had been missed in the PAO1 genome annotation, and which appeared to encode the antitoxin member of a ParDE-like TA system (PA0728.1, **Fig. 2**). However, we did not identify expression evidence for the antitoxin MPAO1_22380 (83 aa) with our iPtgxDB, most likely because our dataset (33% of MPAO1 proteins) was not as extensive as that used in a comprehensive proteogenomic study (85% of *Bartonella henselae* proteins) [31], whose complete membrane proteome coverage included expression evidence for all T4SS members [74]. Nevertheless, we observed proteogenomic evidence for gene products missed in the fragmented MPAO1/P1 genome, for new start sites and for single amino acid variations, underlining the potential value of proteogenomics for application in clinical proteomics.

Our proof of principle experiments uncovered several candidates for follow-up studies and illustrated the benefit of the complete MPAO1 genome, which led to the discovery of six general essential genes not contained in the transposon library, and which will allow to identify evolutionary changes that lead to AMR in biofilm by deep sequencing in the future. Having been validated for the generation of reproducible inter-laboratory *P. aeruginosa* biofilm results, a milestone en route to a community standard (see Data Access), the microfluidic platform can be instrumental to investigate other biofilms, notably clinical pathogens and mixed-species biofilms [69]. The upregulation of the H1-T6SS highly relevant for dominance of *P. aeruginosa* [69] implies that our microfluidic chamber should also be

valuable for this extension. Our proposed workflow (**Fig. 7**) with feedback between genotypic and phenotypic assessment of biofilm characteristics can thus be leveraged across the field of biofilm research and helps bridge the gap between genome-wide and reductionist approaches to study phenomena related to biofilm-associated AMR.

Methods

Bacterial growth and genomic DNA extraction

P. aeruginosa strain MPAO1 (originating from the lab of Dr. Barbara Iglewski) was obtained from Prof. Colin Manoil, UW (Seattle, USA) together with the transposon insertion mutant collection of ~5000 mutated genes (9437 strains) [21]. For DNA extraction, the MPAO1 cryoculture was streaked out on 20% BHI solid medium (7.4 g in 1 L water) containing 1.5% agar (both Sigma, Switzerland). Shaken 20% BHI fluid cultures were inoculated from a single colony and grown at 30 °C until mid-exponential phase (OD600 = 0.5). Genomic DNA (gDNA) was extracted with the GeneElute kit (Sigma, Switzerland), following the Gram-negative protocol, including RNase treatment. A study that had analyzed 9331 complete bacterial genomes [29] (NCBI RefSeq, assembly category: 'complete genome'; status Feb. 23, 2018; see their TableS4) reported that 106 *P. aeruginosa* strains have been sequenced completely, which included only two PAO1 strains (and no complete genome of strain MPAO1). 38/106 (36%) had difficult to assemble genomes with repeat pairs greater 10 kilo base pairs (bp).

Sequencing, *de novo* genome assembly and annotation

PacBio SMRT sequencing was carried out on a RS II machine (1 SMRT cell, P6-C4 chemistry). A size selection step (BluePippin) was used to enrich for fragments longer than 10 kb. The PacBio run yielded 105,221 subreads (1,32 Gbp sequence data). Subreads were *de novo* assembled using the SMRT Analysis portal v5.1.0 and HGAP4 [75], and polished with Arrow. In addition, a 2 x 300 bp paired end library (Illumina Nextera XT DNA kit) was sequenced on a MiSeq. Polishing of the assembly with Illumina reads, circularization, start alignment using *dnaA* and final verification of assembly completeness were performed as described previously [76]. The quality of the aligned reads and the final chromosome was assessed using Qualimap [77]. In addition, we checked for any potential large scale mis-assemblies using Sniffles v1.0.8 [78] by mapping the PacBio subreads using NGMLR v0.2.6 [78]. SPAdes v3.7.1 [79] was run on the Illumina data to detect smaller plasmids that might have

been lost in the size selection step. The genome was annotated with the NCBI's prokaryotic genome annotation pipeline (v3.3) [80]. Prophages were identified with Phaster [81]. Detailed annotations for all CDS were computed as described previously [82]; this included assignment to Cluster of Orthologous Groups (COG) categories using eggnog-mapper (v 1.0.3) and EggNOG 4.5, an Interproscan analysis and prediction or /integration of subcellular localizations, lipoproteins, transmembrane helices and signal peptides (for details, see Supplementary **Data 1**).

Comparative genomics of selected PAO1 genomes

The genome of the *P. aeruginosa* PAO1-UW reference strain [2] was compared to our complete MPAO1 genome using the software Roary (v3.8.0) [83] to define core and strain-specific gene clusters as described before [30,83]. A BlastP analysis helped to correctly identify conserved genes with ribosomal slippage (*prfB*; *p*eptide chain release factor B) or that encode a selenocysteine (MPAO1_25645), which otherwise can be misclassified as unique genes; genes of 120 bp or below (17 in MPAO1) were not considered. ProgressiveMauve [84] was used to align the genomes globally and to identify larger genomic differences. Smaller differences (indels, single nucleotide polymorphisms (SNPs)), were identified and annotated against the PAO1 reference strain as described previously [82]. Furthermore, contigs from the MPAO1/P1 genome [32] were aligned to our complete MPAO1 genome assembly using BWA mem [85]. Bedtools v2.16.1 'genomecov' [86] was used to calculate a gene-wise coverage, allowing to identify genes that were missed in the 140 contigs.

Re-mapping of Transposon sequencing data

MPAO1 Tn-seq datasets [24] were downloaded from NCBI's SRA (SRP052838) and mapped back both to the PAO1-UW reference strain genome [2] and to our MPAO1 assembly following the scripts and notes provided in the Supplement. Insertion sites were computed as described by the authors, reads mapping to multiple genome positions were assigned randomly, and the number of insertion sites per gene was used to differentiate essential and

non-essential genes as described [24]. Genes with zero insertions were considered essential; for the remaining genes, normalized read counts across all insertion sites per gene (considering insertions falling within 5-90% of the length of each gene) were log2 transformed and fitted to a normal distribution. Genes with a *p* value < 0.001 were added to the list of essential genes. Finally, essential and conditionally essential genes were identified among the three main growth conditions (LB medium, minimal medium, sputum) as described [24]. Data from each growth condition consisted of multiple mutant pools; for LB, two mutant pools additionally contained multiple replicates (LB-1: 3 replicates; LB-2: 2 replicates). For LB, genes were considered essential in the mutant pool LB-1 and LB-2 if at least two of three (LB-1) and one of two replicates (LB-2) agreed. Next, a consensus set of essential genes in LB and minimal medium was derived from those genes that were essential in at least two of three mutant pools (LB-1, LB-2 and LB-3) in LB and minimal respectively. Similarly, essential genes in sputum (four mutant pools) were derived if data from at least three of four pools agreed. Finally, genes that were essential in all three growth conditions were called “general essential genes (312)” and genes essential to a specific growth condition were called “condition specific essential genes”. Together, they comprise “all essential genes (577)”; for further details, see Supplement.

Microfluidic chamber used for biofilm growth

The standardized microfluidic flow chamber consisted of a PDMS chip with a straight microfluidic channel (30 mm length x 2 mm width x 0.200 mm depth) that naturally adhered onto a glass coverslip (26 x 60 mm; thickness no.1). The wafer master was fabricated using SU-8 spin-coated to a thickness of 200 μm on a silicon wafer in advance of standard soft lithography replication into PDMS [84]. From this, polyurethane clones of the structures were prepared to upscale production and for sharing microfluidic molds between laboratories. A degassed 10:1 mixture of Sylgard 184 PDMS base and curing agent were cured in an oven at 60 °C for 2 h. Following cooling and retrieval from the SU-8 wafer the structured PDMS was attached, structures facing upwards, to a silicone baking mold using transparent double-

sided adhesive (3M). The PDMS part was degassed, while the two-component polyurethane (Smooth-Cast™ 310) solutions were each thoroughly shaken for 10 min and then combined in a 1:1 ratio followed by thorough mixing (by repeat inversion and then shaking). The PDMS device was then submerged in the mixture, with degassing for 10 min, after which the mold was left overnight in a well ventilated area followed by a hard bake at 60 °C for 4 h. Once cooled the PDMS device was retrieved leaving the polyurethane mold in readiness for replica molding fresh PDMS devices again at 60 °C for 2 h. Importantly, PDMS devices are only retrieved after the polyurethane mold has cooled to room temperature to allow the repeated replication (> 100 times) of precision PDMS microfluidic chambers. Inlet and outlet ports were prepared using 1-mm-diameter biopsy punches (Miltex™) and then the device was enclosed using a coverslip that was cleaned with 2% RBS 35 detergent (prepared in demineralized water), rinsed with tap water, then immersed in 96% ethanol and sonicated for 5 min, followed by a final rinse with demineralized water and then autoclaved. The inlet and outlet of the microfluidic flow chamber were connected to a syringe pump with a 25G needle and waste container, respectively, via sterile PTFE tubing (Smiths Medical, ID 0.38 mm, OD 1.09 mm). The chamber was disinfected by flowing 70% ethanol for 15 min at a rate of 20 µL/min, before rinsing with sterile PBS for 15 min and then flushing with M9 minimal medium (Formedium Ltd, Hunstanto, England) for another 15 min at the same flow rate.

Device inoculation, biofilm staining and confocal laser microscopy

P. aeruginosa MPAO1 was inoculated with 500 µL of an M9-grown overnight pre-culture and grown for ~16-18 h in 10 mL M9 medium (1x M9 salts supplemented with 2 mM $MgSO_4$, 100 µM $CaCl_2$ and 5 mM glucose) at 37 °C with gentle rotation (150 rpm) until a cell concentration of 1.5 x 10^9 bacteria/mL was reached. One mL of the culture was then washed twice with PBS (pH 7.0) by centrifugation at 5,000 xg for 5 min at 10 °C. The bacterial pellet was re-suspended and diluted in PBS + 2% M9 such that the final cell suspension contained 3 x 10^8 bacteria/mL. The microfluidic chamber was set on a hotplate at 37 °C with the glass coverslip in direct contact with the hotplate surface. Freshly prepared bacterial suspension

was flown through at a rate of 5 µL/min for 1 h. After 1 h, the bacterial suspension was replaced by M9 medium and run through the system at 5 µL/min for 72 h. After 72 h, CLSM images were taken. The biofilm was stained by flowing 1 mL of Live/Dead (Life Technologies, Oregon, USA) staining solution (1.5 µL Syto9 + 1.5 µL propidium iodide in 1 mL of sterile demineralized water) through the flow chamber at 5 µL/min. Once the channel was filled, the flow was stopped and the biofilm kept in the dark for 30 min to allow dye penetration. Finally, PBS was flown through the system at 5 µL/min for 30 min to remove the staining agent. Confocal imaging was performed using a Leica SP8 with x63 oil immersion lens (HC PL APO CS2 63x/1.30, Southampton; LabA), a Leica SP8 with x63 water immersion lens (HC PL APO 63x/1.20W CORR CS2; BAM, LabB), and a Leica SP2 with x63 water lens (HCX APO L 63x/0.9W; Groningen, LabC) for 3 biological repeats comprising 3 technical repeats per site (n=9 biological / n=27 technical). Z-stacks (1 µm) were taken of the biofilms formed on the PDMS surface of the device at five separate regions (beside the inlet, 25%, 50%, 75%, and beside the outlet). COMSTAT 2.1 (Image J) analysis of combined confocal data was performed to provide a quantification of average biofilm thickness and Live/Dead biovolume [87]. A 2-way ANOVA multiple comparison was performed with Tukey's post hoc test to determine 95% confidence intervals. Similar conditions were applied to strain PA4726 (*cbrB*) that had shown reduced biofilm growth during screening, and PA3552 (*arnB*) which demonstrated robust biofilm formation. Biofilm formation of both mutant strains was compared to the MPAO1 WT strain after 18 h growth in the flow chamber.

Screening the public MPAO1 transposon library for antibiotic resistance

The protocol to assess the antibiotic resistance of biofilm-forming MPAO1 cells was adapted from a previous study [88]. Frozen mutant stocks of 95 randomly selected mutants of the UW Genome Center's *P. aeruginosa* PAO1 transposon mutant library [21], each harboring a transposon insertion inactivating the function of the respective gene, were allowed to recover in 20% BHI overnight at 150 rpm and 37 °C. All subsequent incubations were done at 37 °C in 96 well plates (TPP tissue culture 96 well plates, Z707902, Sigma-Aldrich) covered with an

air-permeable foil (Breathe-Easy sealing membrane, Z380059, Sigma-Aldrich) without further shaking. The overnight cultures were diluted 10 fold in M9 medium and 100 µL each was distributed in six plates (1 well/mutant/plate). After 24 h incubation, the biofilm formation from two plates was quantified by crystal violet staining, while biofilms from the other four plates were washed with 0.9% NaCl to remove planktonic bacteria. Bacteria were then exposed to either M9 or M9 supplemented with 25 µg/mL of colistin, i.e., much higher than the minimal inhibitory concentration (MIC) for planktonic growth of *P. aeruginosa* (4 µg/mL), allowing us to focus specifically on the biofilm bacteria. After 24h treatment, the medium was removed, biofilms were washed with 0.9% NaCl to remove all traces of antibiotics, and bacteria were allowed to recover in fresh colistin-free M9 medium. After 24 h incubation, the recovery of biofilm bacteria was measured by turbidity (OD600) to reveal if the mutation influences the resistance attributed by the biofilm. To confirm the reliability of our screening, promising mutants were analyzed independently in triplicate. Cell suspensions of each mutant were prepared in M9 medium (5 x10^6 CFU/mL) and biofilm biomass was quantified by crystal violet after 24 h incubation at 37 °C. Biofilm cells resistance was quantified by measuring the turbidity of biofilm suspension after 24 h treatment with different concentrations of colistin and after 24 h recovery in fresh M9 medium. Selected mutants of interest were further characterized to assess biofilm formation (as described above), MIC and MBIC (see Supplementary **Fig. S3** for detail).

Protein extraction from MPAO1 planktonic and biofilm cultures

For planktonic protein extractions, 10 mL MPAO1 was grown overnight (~18 h) in M9 medium under gentle rotation (150 rpm), centrifuged at 4,000 xg/5 min/RT, and the pellet resuspended in 1 mL Hanks' Balanced Salt Solution (HBSS). Biofilms were grown for 72 h using the microfluidic device as previously described, the PDMS device removed from the glass coverslip, and the combined biofilm biomass from 3 lanes harvested into 1 mL HBSS. Cells from both populations were washed twice in HBSS at 10,000 xg/5 min/RT and the pellets resuspended in 1 mL lysis buffer (7 M urea, 2 M thiourea, 35 mM CHAPS, 20 mM

DTT, 1 M NaCl). Samples were frozen at -80 ^{o}C for 30 min and then thawed at 34 ^{o}C for 20 min. Trichloroacetic acid (TCA) precipitation was performed by adding the bacterial samples to 100% ice-cold acetone and 100% trichloroacetic acid in a 1:8:1 ratio and precipitating at -20 ^{o}C for 1 h. Samples were then centrifuged (18,000 xg/10 min/4 ^{o}C), the supernatant discarded, and the pellet washed twice with 1 mL ice-cold acetone (18,000 xg/10 min/4 ^{o}C). Acetone was removed, the pellet air-dried at room temperature, and resuspended in 0.1 M Triethylammonium bicarbonate (TEAB) plus 0.1% Rapigest. Protein sample validation was performed by 1DE gel electrophoresis. 19.5 μL sample was added to 7.5 μL NuPAGE LDS buffer and 3 μL NuPAGE reducing reagent, heated at 70 ^{o}C for 10 min, then run on a NuPAGE 4-12% Bis-Tris gel with MOPS buffer at 200 V for 50 min alongside a Novex Sharp standard. The gel was stained with SimplyBlue Safe Stain for 1 h, then destained with dH_2O.

Protein processing, mass spectrometry and database search

Protein samples were heated at 80 ^{o}C for 10 min, then DTT added at a final concentration of 2 mM and incubated at 60 ^{o}C for 45 min. Samples were then briefly vortexed, pulse spun, and cooled to room temperature before adding iodoacetamide to a final concentration of 6 mM. Samples were incubated at room temperature for 45 min (protected from light), vortexed and pulse spun briefly, then trypsin added at a final concentration of 1.3 μg/mL. Following incubation overnight at 37 ^{o}C (protected from light), trifluoroacetic acid (TFA) was added to a final concentration of 0.5% then incubated at 37 ^{o}C for 30 min. Samples were centrifuged at 13,000 xg for 10 min at RT, the supernatants removed and vacuum concentrated. The resultant pellets were resuspended in 3% acetonitrile + 0.1% trifluoroacetic acid and peptide quantification performed using the Direct Detect system (Merck Millipore). Protein samples were normalized then vacuum concentrated in preparation for mass spectrometry.

Peptide extracts (1 μg on column) were separated on an Ultimate 3000 RSLC nano system (Thermo Scientific) using a PepMap C18 EASY-Spray LC column, 2 μm particle size, 75 μm x 75 cm column (Thermo Scientific) over a 140 min (single run) linear gradient of 3–25% buffer B (0.1% formic acid in acetonitrile (v/v)) in buffer A (0.1% formic acid in water (v/v)) at

a flow rate of 300 nL/min. Peptides were introduced using an EASY-Spray source at 2000 V to a Fusion Tribrid Orbitrap mass spectrometer (Thermo Scientific). The ion transfer tube temperature was set to 275°C. Full MS spectra were recorded from 300 to 1500 m/z in the Orbitrap at 120,000 resolution using TopSpeed mode at a cycle time of 3 s. Peptide ions were isolated using an isolation width of 1.6 amu and trapped at a maximal injection time of 120 ms with an AGC target of 300,000. Higher-energy collisional dissociation (HCD) fragmentation was induced at an energy setting of 28 for peptides with a charge state of 2–4. Fragments were analysed in the Orbitrap at 30,000 resolution. Analysis of raw data was performed using Proteome Discoverer software (Thermo Scientific) and the data processed to generate reduced charge state and deisotoped precursor and associated product ion peak lists. These peak lists were searched against the P. aeruginosa MPAO1 protein database (a max. of one missed cleavage was allowed for tryptic digestion, variable modification was set to contain oxidation of methionine and N-terminal protein acetylation, and carboxyamidomethylation of cysteine was set as a fixed modification). The FDR was estimated with randomized decoy database searches and was filtered to below 1% FDR at the protein level. Differentially abundant proteins were identified using DESeq2 [89]; significantly differentially abundant proteins had an adjusted (multiple testing corrected) *p* value ≤ 0.05 and a $\log_2$ fold change of ≥ 1 or ≤ -1.

Proteogenomics

An iPtgxDB was created for *P. aeruginosa* MPAO1 as described previously [31], using the NCBI annotation as anchor annotation. *Ab initio* gene predictions from Prodigal [90] and ChemGenome [91] and a modified *in silico* prediction that considers alternative start codons (TTG, GTG, CTG) and ORFs above 6 amino acids (aa) in length were integrated in a step-wise fashion. Proteomics data from MPAO1 cells grown planktonically or as biofilm were searched against this iPtgxDB with MS-GF+ (v2019.04.18) [92] using Cysteine carbamidomethylation as fixed, and oxidation of methionine as variable modifications. Using the target-decoy approach of MS-GF+, the FDR at the PSM level was estimated and filtered

below 0.2%. Only unambiguous peptides as identified by a PeptideClassifier analysis [55], using the extension that supports proteogenomics for prokaryotes [31], were considered. The article was previously published as a preprint [93].

Code Availability

Open source R code used for genomic, Tn-seq and proteomics data processing is available from the authors upon request.

Data Availability

The MPAO1 genome sequence is available at NCBI Genbank (acc# CP027857; Bioproject: PRJNA438597, Biosample: SAMN08722738). Read data are available under SRR10153205 (Illumina) and SRR10153206 (PacBio). Proteomics data are available from PRIDE (acc# PXD017122) upon acceptance of the manuscript. The iPtgxDBs for *P. aeruginosa* MPAO1 and PAO1 are available from https://iptgxdb.expasy.org, both as a searchable protein database (FASTA format) and a GFF file, which can be loaded in a genome viewer and overlaid with experimental evidence. Biofilm growth data from the microfluidic chamber will be made available at https://doi.org/10.21253/DMU.c.4851483. To support technology dissemination, the polyurethane master molds of the microfluidic chambers are available upon request from the UoS/NBIC; a CAD file can be found as Supplementary **Data 5**. Code availability: all analyses presented rely on open source software or published code that is referenced.

Acknowledgements

The authors thank Jürg Frey and Daniel Frei (Agroscope) for generating Illumina MiSeq data. The authors acknowledge funding from the Joint Programming Initiative on AntiMicrobial Resistance (JPIAMR) and national grants to JSW for RNA (MRC MR/R005621/1), HvdM for OCO (ZonMW grant #547001003), QR and MTB for JV (SNSF grant 40AR40_173611), and to FS for FP (BMBF #01KI1710). CHA acknowledges funding for ARV through grants 156320 and 197391 from the SNSF. JSW and RNA would also like to thank Mark Willet and the Southampton Imaging and Microscopy Centre for support in performing biofilm imaging.

Competing Interests

The authors declare no competing interests (neither financial nor non-financial).

Author contributions

VS and ARV carried out genome assembly. ARV performed comparative genomics analyses, remapped existing Tn-seq data, created the iPtgxDB, performed proteogenomics analyses and created figures with CHA. MTB grew cells and extracted gDNA. JDPV devised and carried out the screening approach, overseen by QR. OCO and HvdM designed the mold for the microfluidic flow chamber and JW provided device replication expertise. Microfluidic-confined biofilm growth and confirmed reproducibility were undertaken by RNA,

JSW, OCO, HvdM, FP and FS. PS generated shotgun proteomics data from planktonic and biofilm cells provided by RNA. RNA and JSW carried out biofilm growth in the mold for selected mutants from the transposon mutant collection and analyzed proteomics data. CHA oversaw genome sequencing and assembly, comparative genomics and proteogenomics, and wrote the manuscript together with input from RNA, FS, JV, ARV and all other authors. ARV, RNA and JDPV share co-first authorship.

References

1 Moradali, M. F., Ghods, S. & Rehm, B. H. *Pseudomonas aeruginosa* Lifestyle: A Paradigm for Adaptation, Survival, and Persistence. *Front Cell Infect Microbiol* **7**, 39, doi:10.3389/fcimb.2017.00039 (2017).

2 Stover, C. K. *et al.* Complete genome sequence of *Pseudomonas aeruginosa* PAO1, an opportunistic pathogen. *Nature* **406**, 959-964, doi:10.1038/35023079 (2000).

3 Costerton, J. W., Stewart, P. S. & Greenberg, E. P. Bacterial biofilms: a common cause of persistent infections. *Science* **284**, 1318-1322 (1999).

4 Mah, T. F. & O'Toole, G. A. Mechanisms of biofilm resistance to antimicrobial agents. *Trends Microbiol* **9**, 34-39 (2001).

5 Livermore, D. M. Multiple mechanisms of antimicrobial resistance in *Pseudomonas aeruginosa*: our worst nightmare? *Clin Infect Dis* **34**, 634-640, doi:10.1086/338782 (2002).

6 Partridge, S. R., Kwong, S. M., Firth, N. & Jensen, S. O. Mobile Genetic Elements Associated with Antimicrobial Resistance. *Clin Microbiol Rev* **31**, pii: e00088-00017, doi:10.1128/CMR.00088-17 (2018).

7 Lister, P. D., Wolter, D. J. & Hanson, N. D. Antibacterial-resistant *Pseudomonas aeruginosa*: clinical impact and complex regulation of chromosomally encoded resistance mechanisms. *Clin Microbiol Rev* **22**, 582-610, doi:10.1128/CMR.00040-09 (2009).

8 Fernandez, L. & Hancock, R. E. Adaptive and mutational resistance: role of porins and efflux pumps in drug resistance. *Clin Microbiol Rev* **25**, 661-681, doi:10.1128/CMR.00043-12 (2012).

9 Li, X. Z., Plesiat, P. & Nikaido, H. The challenge of efflux-mediated antibiotic resistance in Gram-negative bacteria. *Clin Microbiol Rev* **28**, 337-418, doi:10.1128/CMR.00117-14 (2015).

10 Boucher, H. W. *et al.* Bad bugs, no drugs: no ESKAPE! An update from the Infectious Diseases Society of America. *Clin Infect Dis* **48**, 1-12, doi:10.1086/595011 (2009).

11 Rice, L. B. Progress and challenges in implementing the research on ESKAPE pathogens. *Infect Control Hosp Epidemiol* **31 Suppl 1**, S7-10, doi:10.1086/655995 (2010).

12 Donlan, R. M. & Costerton, J. W. Biofilms: survival mechanisms of clinically relevant microorganisms. *Clin Microbiol Rev* **15**, 167-193, doi:10.1128/cmr.15.2.167-193.2002 (2002).

13 Hall, C. W. & Mah, T. F. Molecular mechanisms of biofilm-based antibiotic resistance and tolerance in pathogenic bacteria. *FEMS Microbiol Rev* **41**, 276-301, doi:10.1093/femsre/fux010 (2017).

14 Mulcahy, L. R., Burns, J. L., Lory, S. & Lewis, K. Emergence of *Pseudomonas aeruginosa* strains producing high levels of persister cells in patients with cystic fibrosis. *J Bacteriol* **192**, 6191-6199, doi:10.1128/JB.01651-09 (2010).

15 Crabbe, A., Jensen, P. O., Bjarnsholt, T. & Coenye, T. Antimicrobial Tolerance and Metabolic Adaptations in Microbial Biofilms. *Trends Microbiol* **27**, 850-863, doi:10.1016/j.tim.2019.05.003 (2019).

16 Kolpen, M. *et al.* Hyperbaric Oxygen Sensitizes Anoxic *Pseudomonas aeruginosa* Biofilm to Ciprofloxacin. *Antimicrob Agents Chemother* **61**, pii: e01024-01017, doi:10.1128/AAC.01024-17 (2017).
17 Conibear, T. C., Collins, S. L. & Webb, J. S. Role of mutation in *Pseudomonas aeruginosa* biofilm development. *PLoS One* **4**, e6289, doi:10.1371/journal.pone.0006289 (2009).
18 McElroy, K. E. *et al.* Strain-specific parallel evolution drives short-term diversification during *Pseudomonas aeruginosa* biofilm formation. *Proc Natl Acad Sci U S A* **111**, E1419-1427, doi:10.1073/pnas.1314340111 (2014).
19 Chandler, C. E. *et al.* Genomic and Phenotypic Diversity among Ten Laboratory Isolates of *Pseudomonas aeruginosa* PAO1. *J Bacteriol* **201**, pii: e00595-00518, doi:10.1128/JB.00595-18 (2019).
20 Klockgether, J. *et al.* Genome diversity of Pseudomonas aeruginosa PAO1 laboratory strains. *J Bacteriol* **192**, 1113-1121, doi:10.1128/JB.01515-09 (2010).
21 Jacobs, M. A. *et al.* Comprehensive transposon mutant library of *Pseudomonas aeruginosa*. *Proc Natl Acad Sci U S A* **100**, 14339-14344, doi:10.1073/pnas.2036282100 (2003).
22 Gallagher, L. A., Shendure, J. & Manoil, C. Genome-scale identification of resistance functions in *Pseudomonas aeruginosa* using Tn-seq. *MBio* **2**, e00315-00310, doi:10.1128/mBio.00315-10 (2011).
23 Murray, J. L., Kwon, T., Marcotte, E. M. & Whiteley, M. Intrinsic Antimicrobial Resistance Determinants in the Superbug *Pseudomonas aeruginosa*. *mBio* **6**, e01603-01615, doi:10.1128/mBio.01603-15 (2015).
24 Lee, S. A. *et al.* General and condition-specific essential functions of *Pseudomonas aeruginosa*. *Proc Natl Acad Sci U S A* **112**, 5189-5194, doi:10.1073/pnas.1422186112 (2015).
25 Turner, K. H., Wessel, A. K., Palmer, G. C., Murray, J. L. & Whiteley, M. Essential genome of *Pseudomonas aeruginosa* in cystic fibrosis sputum. *Proc Natl Acad Sci U S A* **112**, 4110-4115, doi:10.1073/pnas.1419677112 (2015).
26 Poulsen, B. E. *et al.* Defining the core essential genome of *Pseudomonas aeruginosa*. *Proc Natl Acad Sci U S A* **116**, 10072-10080, doi:10.1073/pnas.1900570116 (2019).
27 Gray, A. N. *et al.* High-throughput bacterial functional genomics in the sequencing era. *Curr Opin Microbiol* **27**, 86-95, doi:10.1016/j.mib.2015.07.012 (2015).
28 Goodwin, S., McPherson, J. D. & McCombie, W. R. Coming of age: ten years of next-generation sequencing technologies. *Nat Rev Genet* **17**, 333-351, doi:10.1038/nrg.2016.49 (2016).
29 Schmid, M. *et al.* Pushing the limits of *de novo* genome assembly for complex prokaryotic genomes harboring very long, near identical repeats. *Nucleic Acids Res* **46**, 8953-8965, doi:10.1093/nar/gky726 (2018).
30 Schmid, M. *et al.* Comparative Genomics of Completely Sequenced *Lactobacillus helveticus* Genomes Provides Insights into Strain-Specific Genes and Resolves Metagenomics Data Down to the Strain Level. *Front Microbiol* **9**, 63, doi:10.3389/fmicb.2018.00063 (2018).
31 Omasits, U. *et al.* An integrative strategy to identify the entire protein coding potential of prokaryotic genomes by proteogenomics. *Genome Res* **27**, 2083-2095, doi:10.1101/gr.218255.116 (2017).
32 Olivas, A. D. *et al.* Intestinal tissues induce an SNP mutation in *Pseudomonas aeruginosa* that enhances its virulence: possible role in anastomotic leak. *PLoS One* **7**, e44326, doi:10.1371/journal.pone.0044326 (2012).
33 Winsor, G. L. *et al.* Enhanced annotations and features for comparing thousands of Pseudomonas genomes in the Pseudomonas genome database. *Nucleic Acids Res* **44**, D646-653, doi:10.1093/nar/gkv1227 (2016).
34 Ross, M. G. *et al.* Characterizing and measuring bias in sequence data. *Genome Biol* **14**, R51, doi:10.1186/gb-2013-14-5-r51 (2013).

35 Manz, B., Volke, F., Goll, D. & Horn, H. Measuring local flow velocities and biofilm structure in biofilm systems with magnetic resonance imaging (MRI). *Biotechnol Bioeng* **84**, 424-432, doi:10.1002/bit.10782 (2003).
36 MacCallum, N. *et al.* Liquid-infused silicone as a biofouling-free medical material. *ACS Biomater Sci Eng* **1**, 43-51, doi:10.1021/abc5000578 (2014).
37 Nishijyo, T., Haas, D. & Itoh, Y. The CbrA-CbrB two-component regulatory system controls the utilization of multiple carbon and nitrogen sources in *Pseudomonas aeruginosa*. *Mol Microbiol* **40**, 917-931 (2001).
38 Clarke, D. M., Loo, T. W., Gillam, S. & Bragg, P. D. Nucleotide sequence of the *pntA* and *pntB* genes encoding the pyridine nucleotide transhydrogenase of *Escherichia coli*. *Eur J Biochem* **158**, 647-653, doi:10.1111/j.1432-1033.1986.tb09802.x (1986).
39 Colvin, K. M. *et al.* The Pel and Psl polysaccharides provide *Pseudomonas aeruginosa* structural redundancy within the biofilm matrix. *Environ Microbiol* **14**, 1913-1928, doi:10.1111/j.1462-2920.2011.02657.x (2012).
40 Goodman, A. L. *et al.* A signaling network reciprocally regulates genes associated with acute infection and chronic persistence in *Pseudomonas aeruginosa*. *Dev Cell* **7**, 745-754, doi:10.1016/j.devcel.2004.08.020 (2004).
41 Petrova, O. E. & Sauer, K. A novel signaling network essential for regulating *Pseudomonas aeruginosa* biofilm development. *PLoS Pathog* **5**, e1000668, doi:10.1371/journal.ppat.1000668 (2009).
42 Fernandez, L. *et al.* Adaptive resistance to the "last hope" antibiotics polymyxin B and colistin in *Pseudomonas aeruginosa* is mediated by the novel two-component regulatory system ParR-ParS. *Antimicrob Agents Chemother* **54**, 3372-3382, doi:10.1128/AAC.00242-10 (2010).
43 McPhee, J. B., Lewenza, S. & Hancock, R. E. Cationic antimicrobial peptides activate a two-component regulatory system, PmrA-PmrB, that regulates resistance to polymyxin B and cationic antimicrobial peptides in *Pseudomonas aeruginosa*. *Mol Microbiol* **50**, 205-217 (2003).
44 Filloux, A., Hachani, A. & Bleves, S. The bacterial type VI secretion machine: yet another player for protein transport across membranes. *Microbiology* **154**, 1570-1583, doi:10.1099/mic.0.2008/016840-0 (2008).
45 Duong, F. *et al.* The AprX protein of *Pseudomonas aeruginosa*: a new substrate for the Apr type I secretion system. *Gene* **262**, 147-153, doi:10.1016/s0378-1119(00)00541-2 (2001).
46 McGuffie, B. A., Vallet-Gely, I. & Dove, S. L. sigma Factor and Anti-sigma Factor That Control Swarming Motility and Biofilm Formation in *Pseudomonas aeruginosa*. *J Bacteriol* **198**, 755-765, doi:10.1128/JB.00784-15 (2015).
47 Zhang, W. *et al.* Extracellular matrix-associated proteins form an integral and dynamic system during *Pseudomonas aeruginosa* biofilm development. *Front Cell Infect Microbiol* **5**, 40, doi:10.3389/fcimb.2015.00040 (2015).
48 Petrova, O. E., Schurr, J. R., Schurr, M. J. & Sauer, K. Microcolony formation by the opportunistic pathogen *Pseudomonas aeruginosa* requires pyruvate and pyruvate fermentation. *Mol Microbiol* **86**, 819-835, doi:10.1111/mmi.12018 (2012).
49 Kuchma, S. L. *et al.* Cyclic-di-GMP-mediated repression of swarming motility by *Pseudomonas aeruginosa*: the *pilY1* gene and its impact on surface-associated behaviors. *J Bacteriol* **192**, 2950-2964, doi:10.1128/JB.01642-09 (2010).
50 Borlee, B. R. *et al. Pseudomonas aeruginosa* uses a cyclic-di-GMP-regulated adhesin to reinforce the biofilm extracellular matrix. *Mol Microbiol* **75**, 827-842, doi:10.1111/j.1365-2958.2009.06991.x (2010).
51 Allsopp, L. P. *et al.* RsmA and AmrZ orchestrate the assembly of all three type VI secretion systems in *Pseudomonas aeruginosa*. *Proc Natl Acad Sci U S A* **114**, 7707-7712, doi:10.1073/pnas.1700286114 (2017).
52 Hachani, A. *et al.* Type VI secretion system in *Pseudomonas aeruginosa*: secretion and multimerization of VgrG proteins. *J Biol Chem* **286**, 12317-12327, doi:10.1074/jbc.M110.193045 (2011).

53 Gaille, C., Reimmann, C. & Haas, D. Isochorismate synthase (PchA), the first and rate-limiting enzyme in salicylate biosynthesis of *Pseudomonas aeruginosa*. *J Biol Chem* **278**, 16893-16898, doi:10.1074/jbc.M212324200 (2003).
54 Kang, D. & Kirienko, N. V. Interdependence between iron acquisition and biofilm formation in *Pseudomonas aeruginosa*. *J Microbiol* **56**, 449-457, doi:10.1007/s12275-018-8114-3 (2018).
55 Qeli, E. & Ahrens, C. H. PeptideClassifier for protein inference and targeted quantitative proteomics. *Nat Biotechnol* **28**, 647-650, doi:10.1038/nbt0710-647 (2010).
56 Flemming, H. C. *et al.* Biofilms: an emergent form of bacterial life. *Nat Rev Microbiol* **14**, 563-575, doi:10.1038/nrmicro.2016.94 (2016).
57 Fraser, C. M., Eisen, J. A., Nelson, K. E., Paulsen, I. T. & Salzberg, S. L. The value of complete microbial genome sequencing (you get what you pay for). *J Bacteriol* **184**, 6403-6405 (2002).
58 De Vrieze, M. *et al.* Linking Comparative Genomics of Nine Potato-Associated Pseudomonas Isolates With Their Differing Biocontrol Potential Against Late Blight. *Front Microbiol* **11**, 857, doi:10.3389/fmicb.2020.00857 (2020).
59 Felnagle, E. A. *et al.* Nonribosomal peptide synthetases involved in the production of medically relevant natural products. *Mol Pharm* **5**, 191-211, doi:10.1021/mp700137g (2008).
60 Gulick, A. M. Nonribosomal peptide synthetase biosynthetic clusters of ESKAPE pathogens. *Nat Prod Rep* **34**, 981-1009, doi:10.1039/c7np00029d (2017).
61 Cotter, P. D., Hill, C. & Ross, R. P. Bacteriocins: developing innate immunity for food. *Nat Rev Microbiol* **3**, 777-788, doi:10.1038/nrmicro1273 (2005).
62 Ghequire, M. G. K. & Ozturk, B. A Colicin M-Type Bacteriocin from *Pseudomonas aeruginosa* Targeting the HxuC Heme Receptor Requires a Novel Immunity Partner. *Appl Environ Microbiol* **84**, doi:10.1128/AEM.00716-18 (2018).
63 Page, R. & Peti, W. Toxin-antitoxin systems in bacterial growth arrest and persistence. *Nat Chem Biol* **12**, 208-214, doi:10.1038/nchembio.2044 (2016).
64 Klausen, M. *et al.* Biofilm formation by *Pseudomonas aeruginosa* wild type, flagella and type IV pili mutants. *Mol Microbiol* **48**, 1511-1524, doi:10.1046/j.1365-2958.2003.03525.x (2003).
65 Weiss Nielsen, M., Sternberg, C., Molin, S. & Regenberg, B. *Pseudomonas aeruginosa* and *Saccharomyces cerevisiae* biofilm in flow cells. *J Vis Exp*, doi:10.3791/2383 (2011).
66 Yeung, A. T., Bains, M. & Hancock, R. E. The sensor kinase CbrA is a global regulator that modulates metabolism, virulence, and antibiotic resistance in *Pseudomonas aeruginosa*. *J Bacteriol* **193**, 918-931, doi:10.1128/JB.00911-10 (2011).
67 Dietrich, L. E. *et al.* Bacterial community morphogenesis is intimately linked to the intracellular redox state. *J Bacteriol* **195**, 1371-1380, doi:10.1128/JB.02273-12 (2013).
68 Jiang, F. *et al.* The *Pseudomonas aeruginosa* Type VI Secretion PGAP1-like Effector Induces Host Autophagy by Activating Endoplasmic Reticulum Stress. *Cell Rep* **16**, 1502-1509, doi:10.1016/j.celrep.2016.07.012 (2016).
69 Cheng, Y. *et al.* Population dynamics and transcriptomic responses of *Pseudomonas aeruginosa* in a complex laboratory microbial community. *NPJ Biofilms Microbiomes* **5**, 1, doi:10.1038/s41522-018-0076-z (2019).
70 Varadarajan, A. R. *et al.* A Proteogenomic Resource Enabling Integrated Analysis of Listeria Genotype-Proteotype-Phenotype Relationships. *J Proteome Res* **19**, 1647-1662, doi:10.1021/acs.jproteome.9b00842 (2020).
71 Hood, R. D. *et al.* A type VI secretion system of *Pseudomonas aeruginosa* targets a toxin to bacteria. *Cell Host Microbe* **7**, 25-37, doi:10.1016/j.chom.2009.12.007 (2010).
72 Storz, G., Wolf, Y. I. & Ramamurthi, K. S. Small proteins can no longer be ignored. *Annu Rev Biochem* **83**, 753-777, doi:10.1146/annurev-biochem-070611-102400 (2014).

73 Impens, F. *et al.* N-terminomics identifies Prli42 as a membrane miniprotein conserved in Firmicutes and critical for stressosome activation in *Listeria monocytogenes*. *Nat Microbiol* **2**, 17005, doi:10.1038/nmicrobiol.2017.5 (2017).
74 Omasits, U. *et al.* Directed shotgun proteomics guided by saturated RNA-seq identifies a complete expressed prokaryotic proteome. *Genome Res* **23**, 1916-1927, doi:10.1101/gr.151035.112 (2013).
75 Chin, C. S. *et al.* Nonhybrid, finished microbial genome assemblies from long-read SMRT sequencing data. *Nat Methods* **10**, 563-569, doi:10.1038/nmeth.2474 (2013).
76 Somerville, V. *et al.* Long-read based *de novo* assembly of low-complexity metagenome samples results in finished genomes and reveals insights into strain diversity and an active phage system. *BMC Microbiol* **19**, 143, doi:10.1186/s12866-019-1500-0 (2019).
77 Okonechnikov, K., Conesa, A. & Garcia-Alcalde, F. Qualimap 2: advanced multi-sample quality control for high-throughput sequencing data. *Bioinformatics* **32**, 292-294, doi:10.1093/bioinformatics/btv566 (2016).
78 Sedlazeck, F. J. *et al.* Accurate detection of complex structural variations using single-molecule sequencing. *Nat Methods* **15**, 461-468, doi:10.1038/s41592-018-0001-7 (2018).
79 Bankevich, A. *et al.* SPAdes: a new genome assembly algorithm and its applications to single-cell sequencing. *J Comput Biol* **19**, 455-477, doi:10.1089/cmb.2012.0021 (2012).
80 Tatusova, T. *et al.* NCBI prokaryotic genome annotation pipeline. *Nucleic Acids Res* **44**, 6614-6624, doi:10.1093/nar/gkw569 (2016).
81 Arndt, D. *et al.* PHASTER: a better, faster version of the PHAST phage search tool. *Nucleic Acids Res* **44**, W16-21, doi:10.1093/nar/gkw387 (2016).
82 Fernandez, N. *et al.* An Integrated Systems Approach Unveils New Aspects of Microoxia-Mediated Regulation in *Bradyrhizobium diazoefficiens*. *Front Microbiol* **10**, 924, doi:10.3389/fmicb.2019.00924 (2019).
83 Page, A. J. *et al.* Roary: rapid large-scale prokaryote pan genome analysis. *Bioinformatics* **31**, 3691-3693, doi:10.1093/bioinformatics/btv421 (2015).
84 Darling, A. E., Mau, B. & Perna, N. T. progressiveMauve: multiple genome alignment with gene gain, loss and rearrangement. *PLoS One* **5**, e11147, doi:10.1371/journal.pone.0011147 (2010).
85 Li, H. Aligning sequence reads, clone sequences and assembly contigs with BWA-MEM. *ArXiv*, 1303.3997v1302 [q-bio.GN] (2013).
86 Quinlan, A. R. & Hall, I. M. BEDTools: a flexible suite of utilities for comparing genomic features. *Bioinformatics* **26**, 841-842, doi:10.1093/bioinformatics/btq033 (2010).
87 Heydorn, A. *et al.* Quantification of biofilm structures by the novel computer program COMSTAT. *Microbiology* **146 (Pt 10)**, 2395-2407, doi:10.1099/00221287-146-10-2395 (2000).
88 Mah, T. F. Establishing the minimal bactericidal concentration of an antimicrobial agent for planktonic cells (MBC-P) and biofilm cells (MBC-B). *J Vis Exp*, e50854, doi:10.3791/50854 (2014).
89 Love, M. I., Huber, W. & Anders, S. Moderated estimation of fold change and dispersion for RNA-seq data with DESeq2. *Genome Biol* **15**, 550, doi:10.1186/s13059-014-0550-8 (2014).
90 Hyatt, D. *et al.* Prodigal: prokaryotic gene recognition and translation initiation site identification. *BMC Bioinformatics* **11**, 119, doi:10.1186/1471-2105-11-119 (2010).
91 Singhal, P., Jayaram, B., Dixit, S. B. & Beveridge, D. L. Prokaryotic gene finding based on physicochemical characteristics of codons calculated from molecular dynamics simulations. *Biophys J* **94**, 4173-4183, doi:10.1529/biophysj.107.116392 (2008).
92 Kim, S. & Pevzner, P. A. MS-GF+ makes progress towards a universal database search tool for proteomics. *Nat Commun* **5**, 5277, doi:10.1038/ncomms6277 (2014).

93 Varadarajan, A. R. *et al.* An integrated model system to gain mechanistic insights into biofilm formation and antimicrobial resistance development in *Pseudomonas aeruginosa* MPAO1. *Preprint at https://doi.org/10.1101/2020.02.06.936690.* (2020).

Figure Legends

Fig. 1. Genome map of *P. aeruginosa* MPAO1 and comparison to other strains.

(**a**) The Circos plot visualizes the comparison of our complete MPAO1 genome (outer circle with genome coordinates) and that of strain MPAO1/P1 (second circle; blue), the respective gaps (third circle; blue) followed by annotated prophages (fourth circle; purple), missing genes (fifth circle, light blue), pseudogenes (sixth circle; brown), and GC skew (seventh circle; positive - purple; negative - green). (**b**) Differences of the MPAO1 genome compared to the PAO1 reference strain. Going from outer towards inner circles, the following genome features are shown: (1) a large inversion (gray) flanked by rRNAs (not shown), (2) SNPs (dark orange), (3) INDELs (light orange) (4) prophages (purple), (5) genes unique to MPAO1 (blue). (**c**) Comparative genomic analysis of *P. aeruginosa* strains MPAO1 and PAO1-UW. The Venn diagram shows the core gene clusters (paralogous genes are grouped into the same cluster provided they belong to a syntenic genomic region) and the respective number of strain-specific CDS clusters.

Fig. 2. An overview of annotated genes in selected prophage regions and their essentiality classification.

MPAO1-unique essential genes are shown in dark blue, general essential MPAO1 genes with a red arrow outline. (**a**) Genes located in prophage region 2 of PAO1-UW (gray), the corresponding inverted region in strain MPAO1 (light blue arrows in middle), and the prophage region 3 (light blue arrows on top) unique to MPAO1 are shown (not drawn to scale), the genomic positions of their boundaries (5' to 3') and flanking tRNAs. Genes connected by lines are orthologous to each other based on comparative genomics combined with a Blast analysis. (**b**) Transposon insertions in selected genes of prophage region 3 of MPAO1. Insertion frequencies in six genes are shown using data mapped from the LB-1 (3 replicates), LB-2 (2 replicates) and LB-3 (1 sample) Tn-seq libraries. Non-essential genes (based on dataset of 577 genes essential in one of three primary growth conditions) are shown in light blue.

Fig. 3. The publicly available mold design for the microfluidic flow chamber allows reproducible biofilm formation as confirmed by an inter-laboratory comparison.
(**a**) Schematic and dimensions of the flow chamber. (**b**) Representative images of 72 h MPAO1 WT biofilms grown on the PDMS surface of the device under laminar flow conditions at five different locations along the channel. Biofilms were treated with live/dead staining (green – live cells stained with Syto9; red – dead cells stained with propidium iodide). Scale bar in confocal XY plane: 40 μm. Sagittal XZ section represents biofilm thickness. (**c**) COMSTAT data for average thickness, and live/dead biovolume of 72 h MPAO1 WT biofilms generated by three different laboratories, with 95% confidence interval comparisons (3 biological repeats comprising 3 technical repeats per site, i.e., n=9 biological / n=27 technical repeats overall; error bars - standard error of mean; 2-way ANOVA with lab and channel location as variables followed by multiple comparisons Tukey test). *p value < 0.05.

Fig. 4. Proof of principle that biofilm growth-relevant and AMR-related genes can be identified in adequate screens using the MPAO1 transposon mutant library.
A diagram of the protocol is shown in Supplementary **Fig. 3**. (**a**) Biofilm formation of 90 MPAO1 mutant strains (X-axis) after 24h incubation in M9 medium (average of two independent wells). Biofilm biomass was quantified by crystal violet. (**b**) Ability of biofilms formed by 90 MPAO1 mutant strains to recover after colistin treatment (see Methods). The recovery of treated biofilm cells was normalized to the recovery of non-treated biofilm cells (defined as 100%). The *arnB* mutant (PA3552) is highlighted in red, as well as the highest biofilm former missing *pntAA* (PA0195) and the lowest biofilm former missing *cbrB* (PA4726).

Fig. 5. Confirmation of the phenotypes identified in our screening.
(**a**) Biofilm formation was quantified after 24h incubation in M9 medium by crystal violet staining (average of at least 18 wells from two independent cultures). The *pslB* and *retS* mutants were used as a reference for low and high biofilm formation, respectively. The *cbrB* and *pntAA* mutants demonstrated substantially reduced and increased biofilm formation,

respectively. Symbols (* and §) indicate significant differences (Student's tests with *p* value < 0.001) in comparison to MPAO1 WT and the *arnB* mutant, respectively. PAO1 genes are shown in brackets, the respective MPAO1 genes are mentioned in the text. (**b**) Resistance of planktonic and biofilm cells towards colistin was evaluated for a subset of mutant strains identified in the screening ([1]) or based on differential proteomics abundance ([2]). The MIC was determined as the lowest concentration resulting in 90% reduction of bacterial growth after 24h in M9 medium compared to the non-treated condition (average of four replicates from two independent cultures). The MBIC was determined as the lowest concentration resulting in 50% or 90% reduction of the biofilm cells recovery after 24h treatment compared to the non-treated condition (average of four replicates from two independent cultures). (**c**) Comparative confocal micrographs after live/dead staining (green – live cells stained with Syto9; red – dead cells stained with propidium iodide) of 18 h MPAO1 WT, *cbrB* and *arnB* biofilms grown under microfluidic conditions using the publicly available mold confirm reduced biofilm formation for the *cbrB mutant* and robust biofilm formation of the *arnB mutant* in the absence of treatment.

Fig. 6. Proteomic experiments identify known biofilm-related proteins and new information. (**a**) Differential protein abundance between MPAO1 mid-exponential planktonic cells and 72 h biofilms. Selected significantly upregulated proteins (red dots) known to play a role in biofilm formation/growth are labeled, proteins downregulated in planktonic growth are shown in blue. Red triangles denote proteins encoded by genes missed in the MPAO1/P1 genome. (**b**) Proteogenomic expression evidence for a longer protein than annotated by RefSeq: the Prodigal predicted protein MPAO1prod_16460 (gray arrow; 447 aa; amino acid) is 44 aa longer than the RefSeq annotated MPAO1_08365 and encodes a glutamine synthetase (blue arrow; 413 aa). The NH-terminal extension is supported by 1 peptide (red) with seven PSMs and harbors a 40 aa longer glutamine synthetase N-terminal domain compared to the RefSeq protein. (**c**) Proteogenomic expression evidence for a single nucleotide insertion (red) in the MPAO1_25975 gene (blue arrow) compared to its PAO1 homolog PA4875

(annotated as pseudogene; gray open arrow). The change is supported by peptide evidence (1 red bar).

Fig. 7. Integrated model system to identify and validate genes relevant for biofilm growth and AMR.

A sequential genomics-driven workflow (blue arrows) to *de novo* assemble the complete genome, identify unique and conserved genes among key reference strains by comparative genomics and missed genes by proteogenomics is integrated with an experimental workflow in the form of an iterative cycle that can be entered at various points (yellow arrows). This workflow allows the study of biofilm grown cells, to explore differentially abundant genes or proteins compared to planktonic cells and to screen mutant libraries to identify functionally relevant genes. The model leverages the enormous value of genetic resources like gene knockout or transposon insertion mutant libraries and functional genomics datasets (RNA-seq, Tn-seq, etc.; blue containers). Additionally, it allows for phenotypic characterization of biofilms formed by mutant strains, thereby allowing us to determine the impact of specific genes on biofilm formation and assess their role in AMR (yellow arrows).

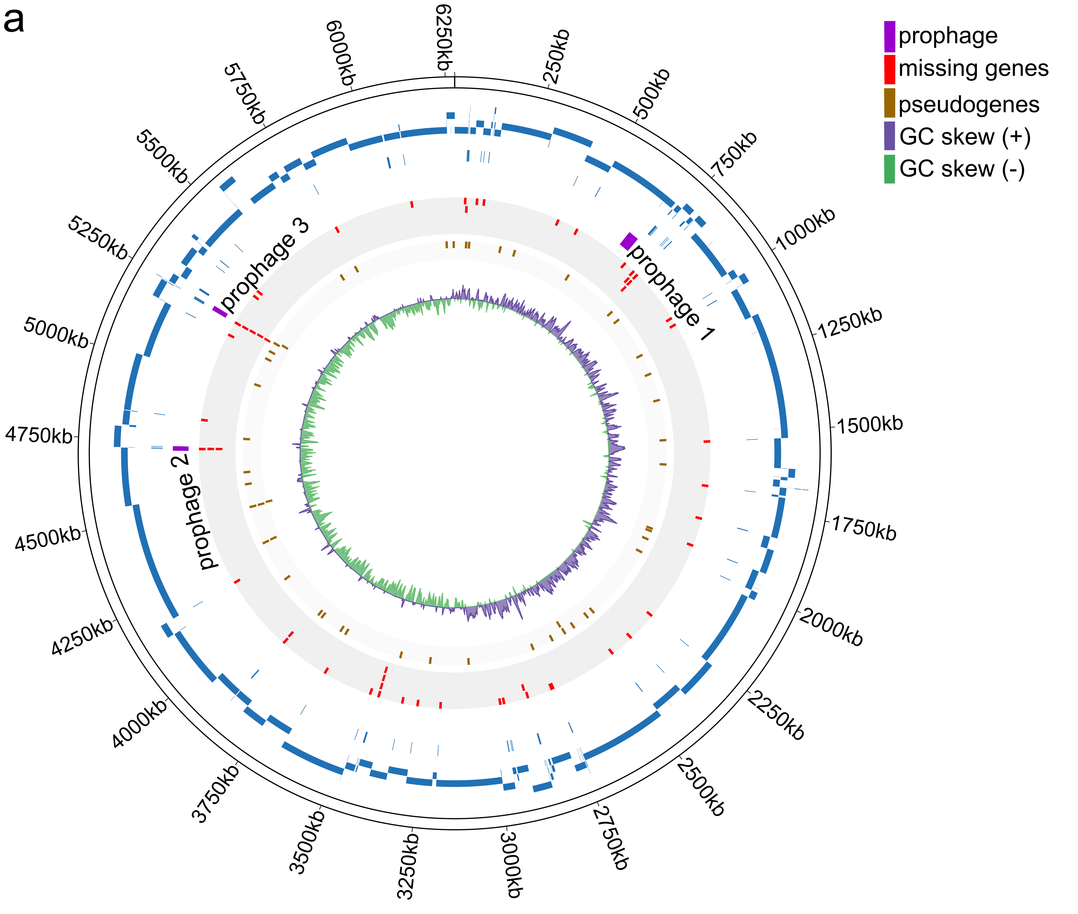
a
prophage
missing genes
pseudogenes
GC skew (+)
GC skew (-)
prophage 1
prophage 2
prophage 3
250kb
500kb
750kb
1000kb
1250kb
1500kb
1750kb
2000kb
2250kb
2500kb
2750kb
3000kb
3250kb
3500kb
3750kb
4000kb
4250kb
4500kb
4750kb
5000kb
5250kb
5500kb
5750kb
6000kb
6250kb

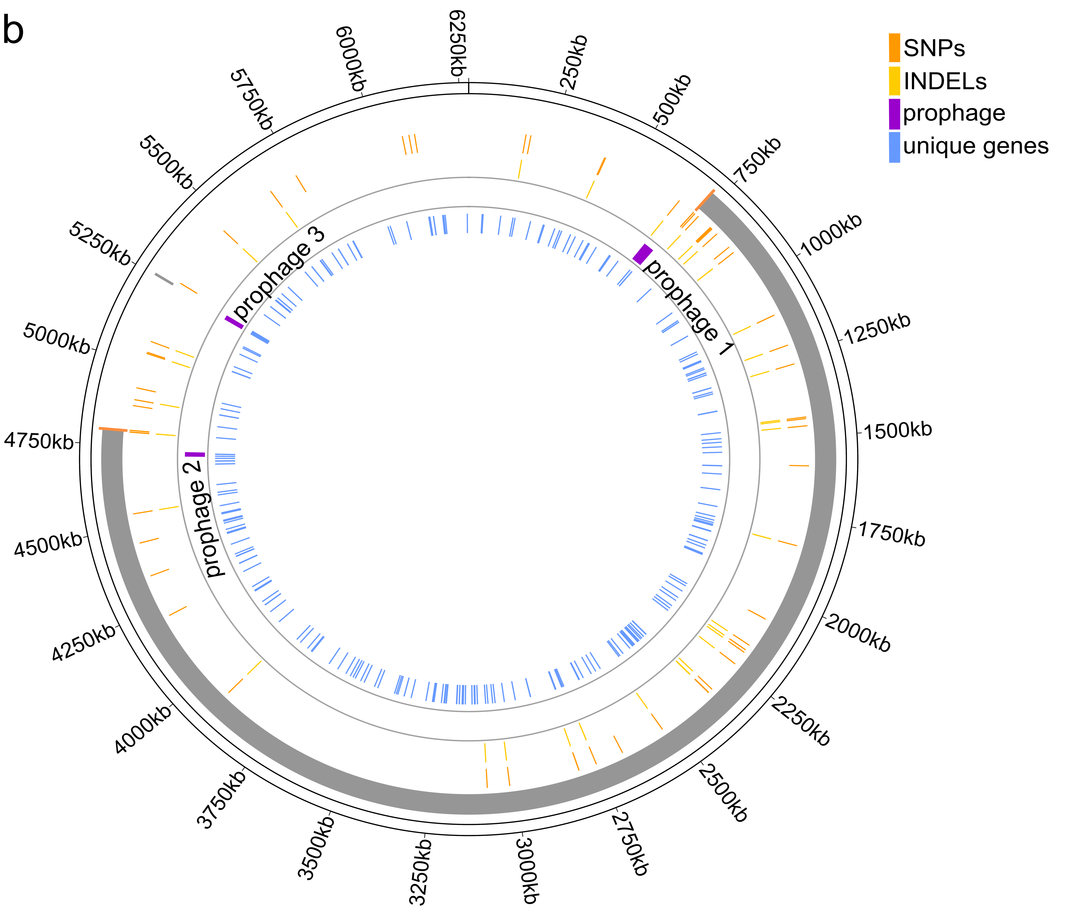
b
SNPs
INDELs
prophage
unique genes
prophage 1
prophage 2
prophage 3
250kb
500kb
750kb
1000kb
1250kb
1500kb
1750kb
2000kb
2250kb
2500kb
2750kb
3000kb
3250kb
3500kb
3750kb
4000kb
4250kb
4500kb
4750kb
5000kb
5250kb
5500kb
5750kb
6000kb
6250kb

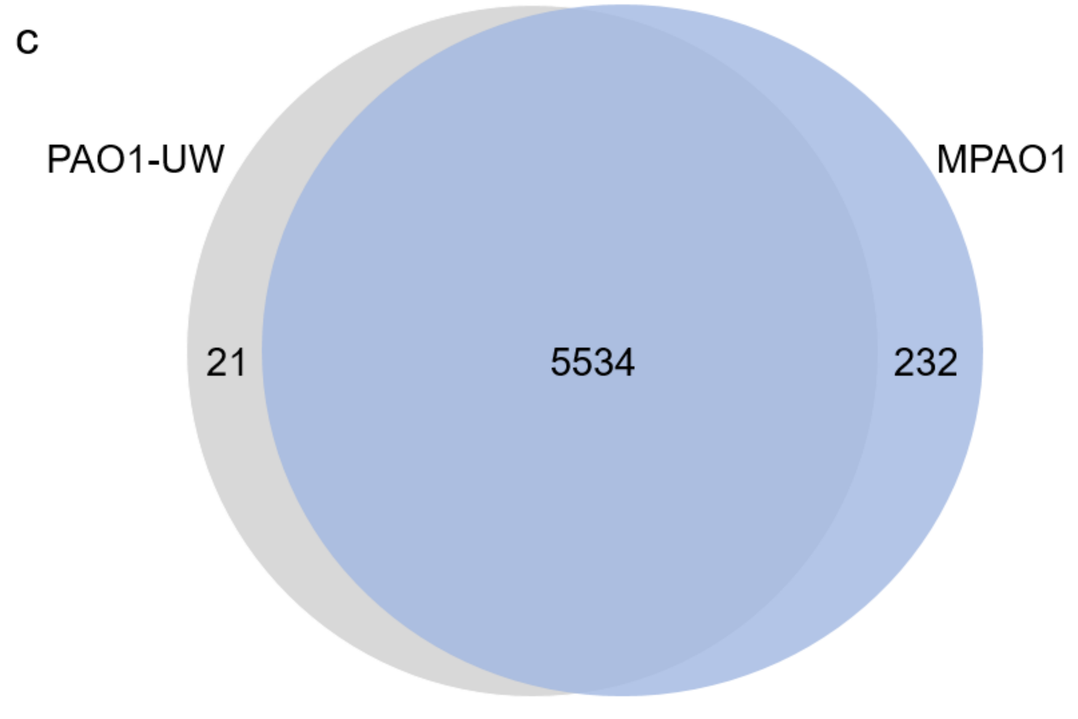
c
PAO1-UW
MPAO1
21
5534
232

a

5,241,813
(tRNA Met)
Prophage 3 (12.8 Kb)
5,254,613
MPAO1
24865
MPAO1
24885
MPAO1
24890
4,717,609
(tRNA Gly)
Prophage 2 (12.3 Kb)
MPAO1
22450
4,730,005
MPAO1
22380
PA0728.1
PA0717
780,995
Prophage 2 (15.7 Kb)
796,776
(tRNA Gly)

b

Genomic
sequence
4,741 bp
5,250,000 bp
5,251,000 bp
5,252,000 bp
5,253,000 bp
5,254,000 bp
LB-1
+500
-500
LB-2
+150
-150
LB-3
+150
-150
MPAO1_24865
MPAO1_24870
MPAO1_24875
MPAO1_24880
MPAO1_24885
MPAO1_24890

a

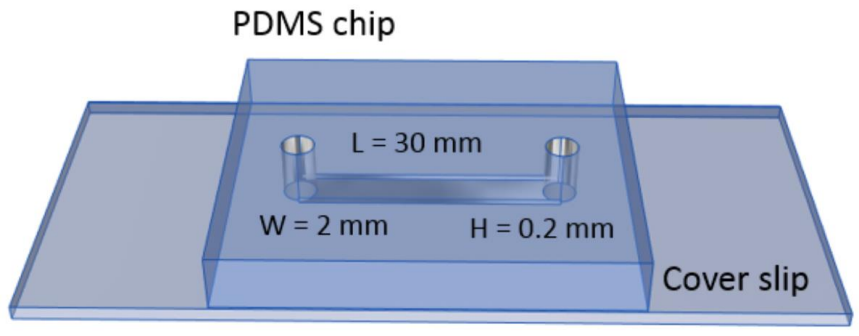
PDMS chip
L = 30 mm
W = 2 mm
H = 0.2 mm
Cover slip

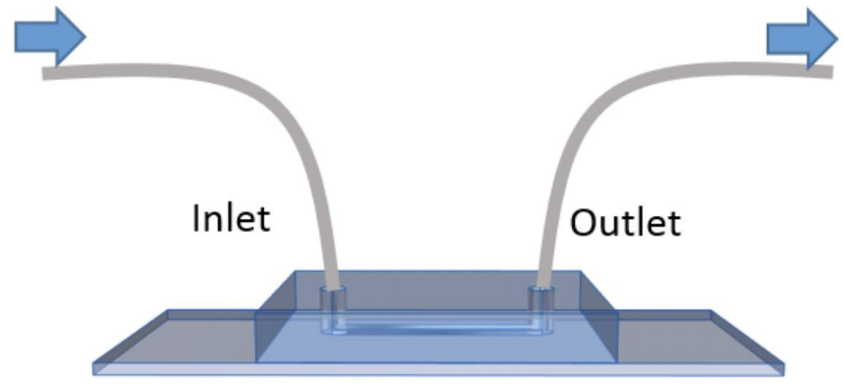
Inlet
Outlet

b

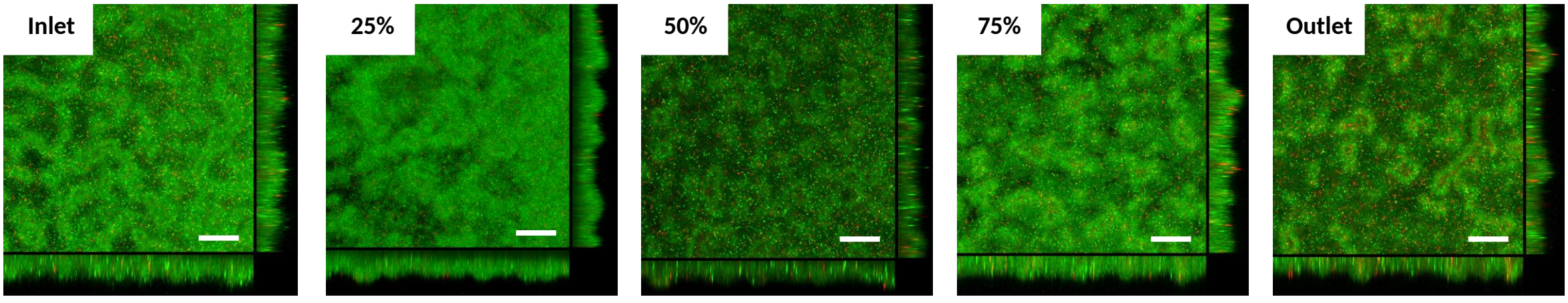
Inlet
25%
50%
75%
Outlet

C

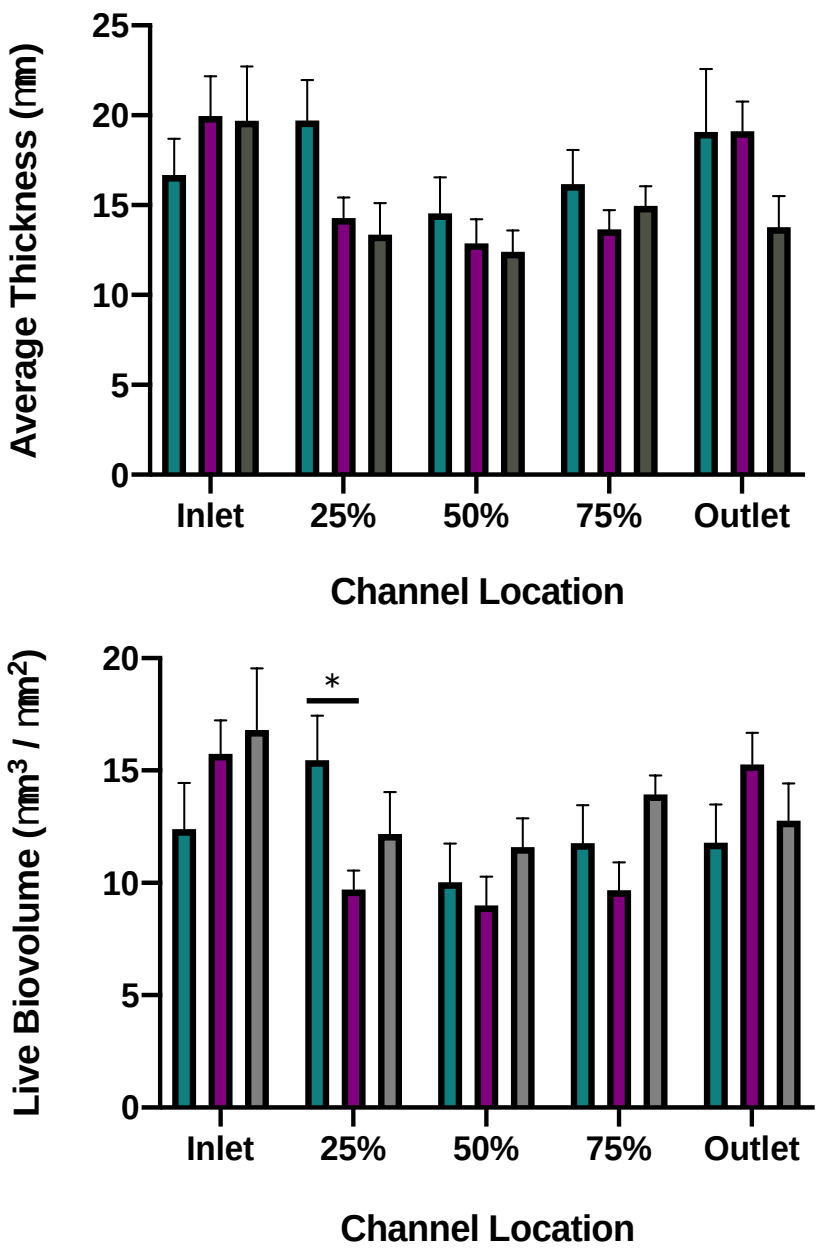
Average Thickness (mm)
Live Biovolume (mm³ / mm²)
Inlet
25%
50%
75%
Outlet
Channel Location
*

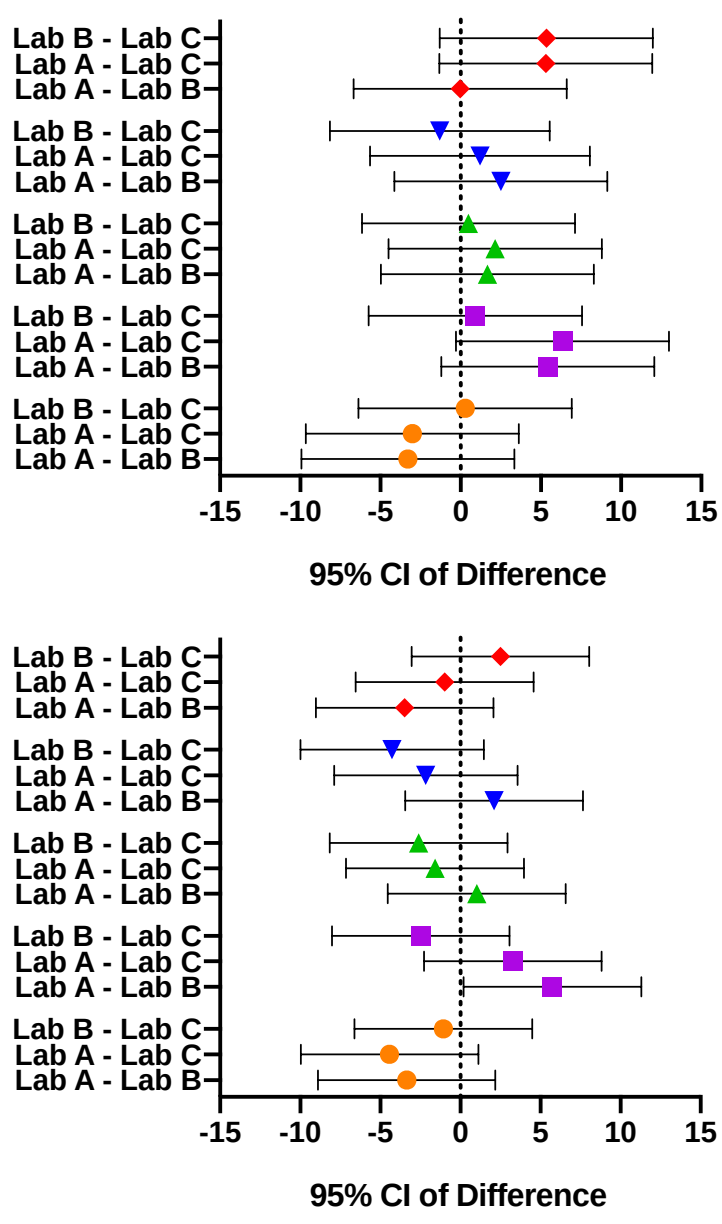
Lab B - Lab C
Lab A - Lab C
Lab A - Lab B
-15
-10
-5
0
5
10
15
95% CI of Difference

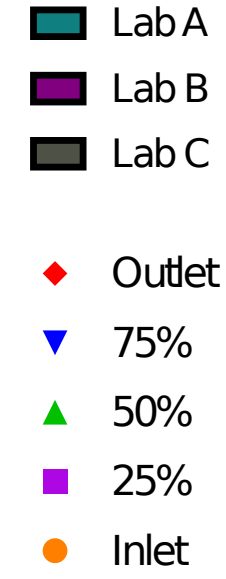
Lab A
Lab B
Lab C
Outlet
75%
50%
25%
Inlet

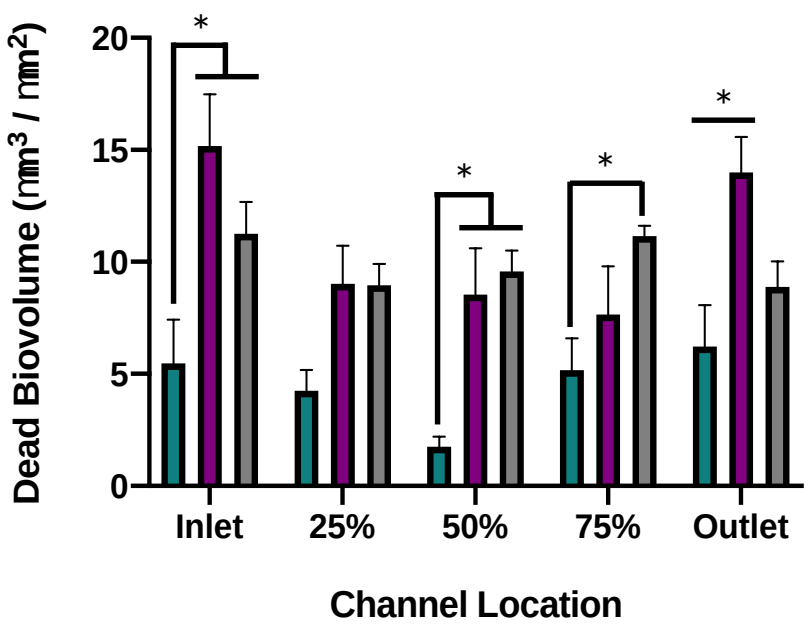
Dead Biovolume (mm³ / mm²)
Inlet
25%
50%
75%
Outlet
Channel Location
*

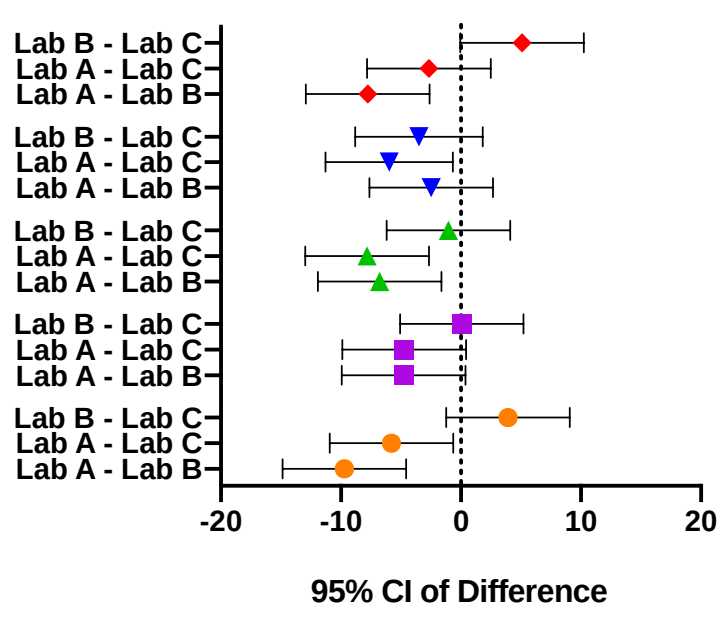
Lab B - Lab C
Lab A - Lab C
Lab A - Lab B
-20
-10
0
10
20
95% CI of Difference

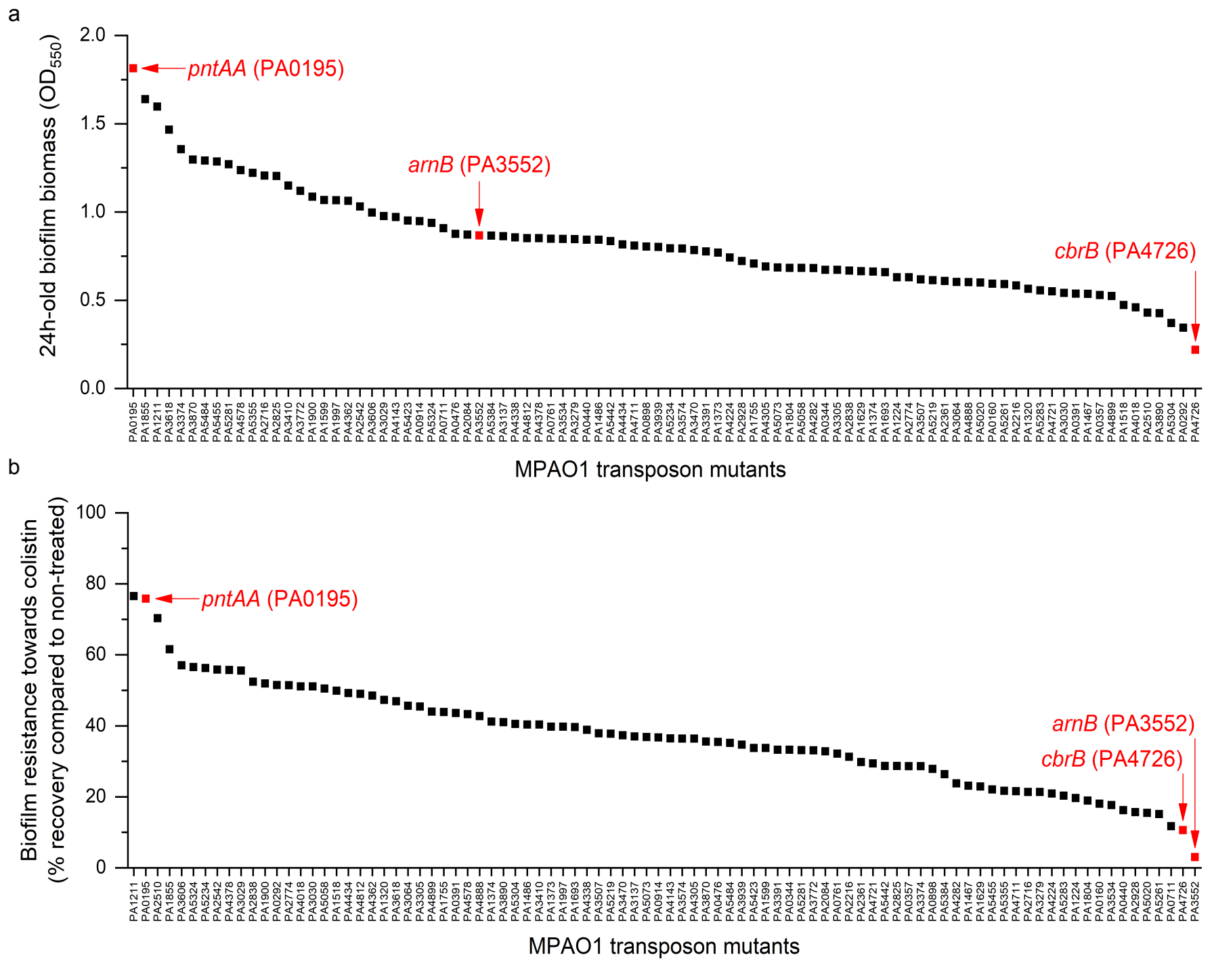
a
24h-old biofilm biomass (OD550)
2.0
1.5
1.0
0.5
0.0
pntAA (PA0195)
arnB (PA3552)
cbrB (PA4726)
PA0195 PA1855 PA1211 PA3618 PA3374 PA3870 PA5484 PA5455 PA5281 PA4578 PA5355 PA2716 PA2825 PA3410 PA3772 PA1900 PA1599 PA1997 PA4362 PA2542 PA3606 PA3029 PA4143 PA5423 PA0914 PA5324 PA0711 PA0476 PA2084 PA3552 PA5384 PA3137 PA4338 PA4812 PA4378 PA0761 PA3534 PA3279 PA0440 PA1486 PA5442 PA4434 PA4711 PA0898 PA3939 PA5234 PA3574 PA3470 PA3391 PA1373 PA4224 PA2928 PA1755 PA4305 PA5073 PA1804 PA5058 PA4282 PA0344 PA3305 PA2838 PA1629 PA1374 PA1693 PA1224 PA2774 PA3507 PA5219 PA2361 PA3064 PA4888 PA5020 PA0160 PA5261 PA2216 PA1320 PA5283 PA4721 PA3030 PA0391 PA1467 PA0357 PA4899 PA1518 PA4018 PA2510 PA3890 PA5304 PA0292 PA4726
MPAO1 transposon mutants
b
Biofilm resistance towards colistin
(% recovery compared to non-treated)
100
80
60
40
20
0
pntAA (PA0195)
arnB (PA3552)
cbrB (PA4726)
PA1211 PA0195 PA2510 PA1855 PA3606 PA5324 PA5234 PA2542 PA4378 PA3029 PA2838 PA1900 PA0292 PA2774 PA4018 PA3030 PA5058 PA1518 PA4434 PA4812 PA4362 PA1320 PA3618 PA3064 PA3305 PA4899 PA1755 PA0391 PA4578 PA4888 PA1374 PA3890 PA5304 PA1486 PA3410 PA1373 PA1997 PA1693 PA4338 PA3507 PA5219 PA3470 PA3137 PA5073 PA0914 PA4143 PA3574 PA4305 PA3870 PA0476 PA5484 PA3939 PA5423 PA1599 PA3391 PA0344 PA5281 PA3772 PA2084 PA0761 PA2216 PA2361 PA4721 PA5442 PA2825 PA0357 PA3374 PA0898 PA5384 PA4282 PA1467 PA1629 PA5455 PA5355 PA4711 PA2716 PA3279 PA4224 PA5283 PA1224 PA1804 PA0160 PA3534 PA0440 PA2928 PA5020 PA5261 PA0711 PA4726 PA3552
MPAO1 transposon mutants

a

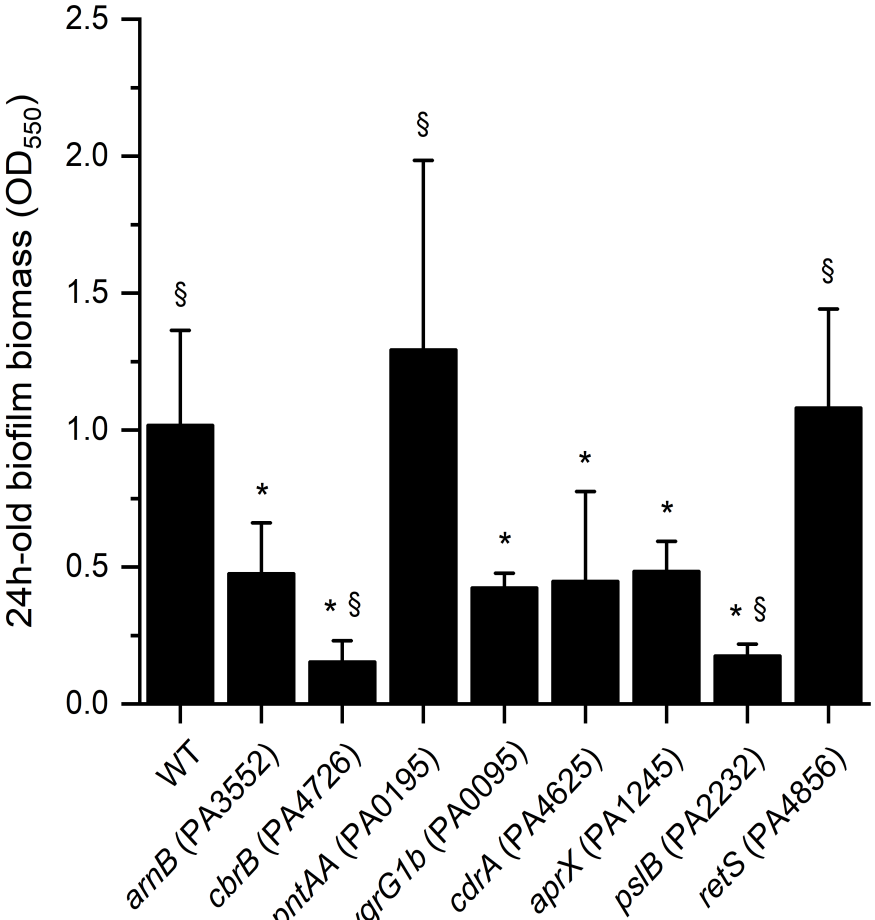

b

Gene inactivated	MIC colistin (µg/mL)	MBIC 50 colistin (µg/mL)	MBIC 90 colistin (µg/mL)
None (WT)	8	50	200
arnB (PA3552)[1]	2	8	12.5
cbrB (PA4726)[1]	2	4	100
pntAA (PA0195)[1]	16	200	>200
vgrG1b (PA0095)[2]	16	100	>200
cdrA (PA4625)[2]	8	50	200
aprX (PA1245)[2]	16	100	>200

Candidates selected from [1]screening and [2]proteomic analysis

c

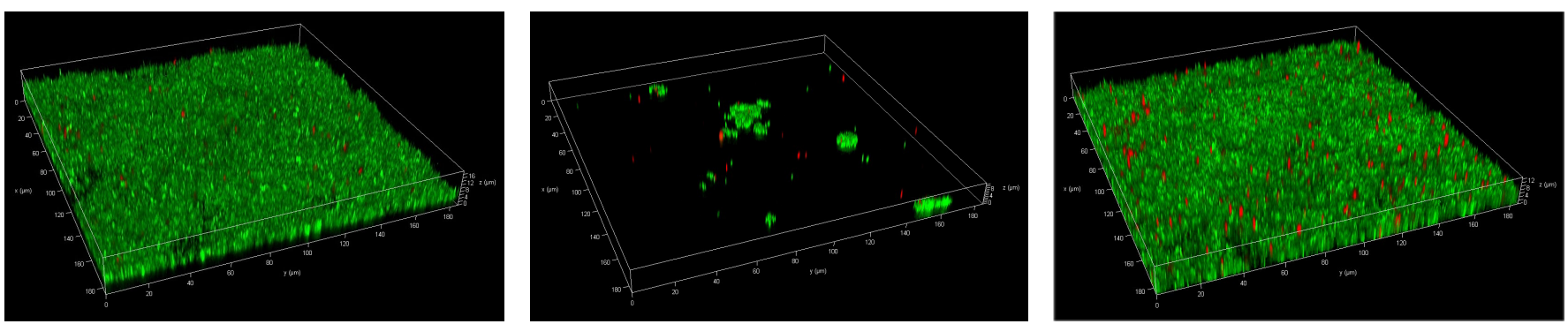

a

upregulated
downregulated

VgrG1b (MPAO1_00520)
MPAO1_19625
CdrA
CdrB
MuiA
CbpD
NirS
AcnA
PilY1
PchA
MPAO1_15475
ArgF
PctC
PiuA

log2(Biofilm/Planktonic)

mean normalized counts

b

4,749 bp
1,746,000 bp
1,747,000 bp
1,748,000 bp
1,749,000 bp
1,750,000 bp
RefSeq
MPAO1_08360
MPAO1_08365
MPAO1_08370
Prodigal
MPAO1prod_16450
MPAO1prod_16460
MPAO1prod_16470
Peptide evidence

c

1,014 bp
5,482,800 bp
5,483,000 bp
5,483,200 bp
5,483,400 bp
5,483,600 bp
MPAO1
AGCGGCTTCG
CDS
MPAO1_25975
MPAO1_25980
Peptide evidence
1,012 bp
5,472,200 bp
5,472,400 bp
5,472,600 bp
5,472,800 bp
5,473,000 bp
PAO1-UW
AGCGCCTTCG
CDS
PA4875
PA4876
Peptide evidence

Robust biofilm growth system

Microfluidic device

Bacterial model organisms

Mutant libraries

Functional genomic data

RNA-seq

Proteomics

Tn-seq

...

Fully resolved genome

De novo assembly

Integration

Phenotype

Genotype, functional elements

Transcriptomics & Proteomics

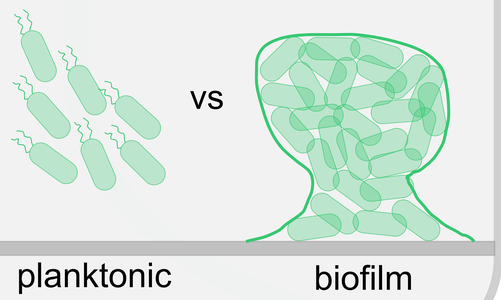

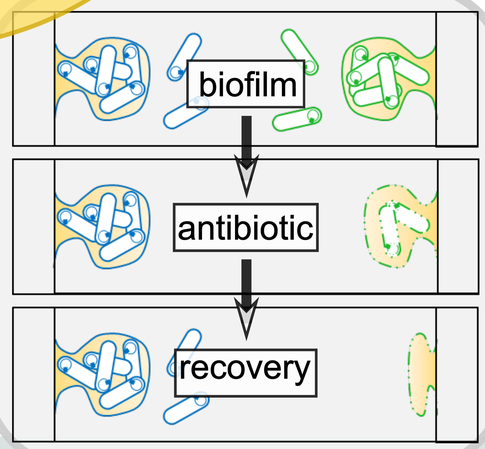

Proteogenomics

RefSeq

+

Prodigal

in silico ORFs

Integrate annotations

iPtgxDB

Comparative genomics

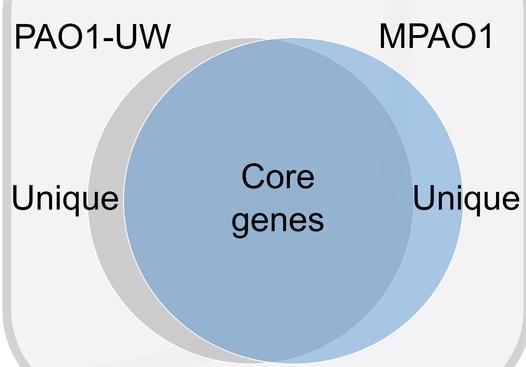

Identify relevant genes

Library screens: biofilm growth & AMR

Identify novel sORFs

Unique / shared genes

Table 1. Summary over core and strain-specific CDS of strains MPAO1 and PAO1-UW.
*All individual CDS are shown including those that are grouped in gene clusters (paralogs) in **Fig. 1c**. **CDS of 120 bp or below are not considered (see Methods).

Category	***P. aeruginosa* MPAO1**	***P. aeruginosa* PAO1-UW**
Total No. of genes	5,926	5,697
Total No. of CDSs	5,799	5,572
No. of core CDSs (clusters*)	5,548 (5,534)	5,545 (5,534)
No. of unique (strain-specific) CDSs (clusters)	234 (232)	19 (21)
Unique ncRNA	-	3
CDSs ≤ 120 bp**	17	5

Table 2. List of 18 selected MPAO1-unique genes along with their essentiality classification in all 16 Tn-seq samples [24] and comments about their genomic location. Information about all MPAO1-unique essential genes is available in Supplementary **Data 4**.

Locus	Gene annotation	General essential	Essential in x/16 samples	Comment
MPAO1_22380	type II toxin-antitoxin system Phd/YefM family antitoxin	yes	16	Prophage 2
MPAO1_00215	hypothetical protein	yes	15	*Operon?
MPAO1_10410	hypothetical protein	yes	14	
MPAO1_22450	DNA-binding protein	yes	14	Prophage 2
MPAO1_25260	cytidine deaminase		12	
MPAO1_12950	hypothetical protein	yes	11	
MPAO1_00230	hypothetical protein		10	*Operon?
MPAO1_20095	hypothetical protein		10	
MPAO1_02335	dihydropyrimidinase		9	
MPAO1_15010	6-O-methylguanine DNA methyltransferase		9	
MPAO1_15215	amino acid permease		9	
MPAO1_18025	ferredoxin		9	
MPAO1_02315	oxidoreductase		8	
MPAO1_05695	hypothetical protein	yes	8	Bacteriocin (GO)
MPAO1_08710	DUF3304 domain-containing protein		8	
MPAO1_10195	universal stress protein		8	
MPAO1_14380	glycosyltransferase		8	
MPAO1_24865	hypothetical protein		8	Prophage 3

Table 3. List of 61 proteins with significant differential abundance (see text) or unique expression when comparing biofilm grown and planktonic cells.
Publications linking the genes/proteins with various roles in biofilms are listed for proteins highlighted in **Fig. 6**. Two genes missed in MPAO1/P1 are shown in bold. Gene names stem from the National Center for Biotechnology Information (NCBI) annotation, or were deduced from the eggNOG annotation or the respective PAO1 homolog (*) or the *Pseudomonas* genome database (**); see also Supplementary **Data 1**.

Locus tag	gene	product	log2 FC	padj	Comment, Reference
Biofilm only					
MPAO1_19985	*napA*	Nitrate reductase catalytic subunit NapA	5.02	0.05	
MPAO1_04195		SH3 domain-containing protein	5.02	0.05	
MPAO1_10705		Methyl-accepting chemotaxis protein	5.11	0.03	
MPAO1_17160		EscC/YscC/HrcC family type III secretion system outer membrane ring protein	5.11	0.03	
MPAO1_21585		Itaconyl-CoA hydratase	5.19	0.04	
MPAO1_17195		Translocator outer membrane protein PopD	5.19	0.02	
MPAO1_17200		Hypothetical protein	5.34	0.01	
MPAO1_00520	***vgrG1b****	**Type VI secretion system tip protein VgrG1b** [52]	**5.41**	**0.01**	H1-T6SS [44]
MPAO1_20935		Beta-keto-ACP synthase	5.61	0.04	
MPAO1_24325		Cytochrome c551 peroxidase	6.11	0.00	
Diff. Abundant					
MPAO1_07815		Osmoprotectant NAGGN system M42 family peptidase	4.70	0.02	
MPAO1_19625	*aprX*	Hypothetical protein	5.45	0.00	[45]
MPAO1_24535	***cdrA****	**Filamentous hemagglutinin N-terminal domain-containing protein**	**6.54**	**0.00**	[50]
MPAO1_02725	*nirF*	Protein NirF	4.30	0.01	
MPAO1_24530	*cdrB**	ShlB/FhaC/HecB family hemolysin secretion/activation protein	4.35	0.01	[50]
MPAO1_25250		BON domain-containing protein	3.28	0.05	
MPAO1_19595		Serralysin	3.75	0.01	
MPAO1_22090	*putA*	Bifunctional proline dehydrogenase/L-glutamate gamma-semialdehyde dehydrogenase PutA	3.00	0.01	
MPAO1_18330	*muiA**	Mucoidy inhibitor MuiA	2.69	0.01	[46]
MPAO1_21730	*cbpD**	Chitin-binding protein CbpD	2.79	0.00	[47]
MPAO1_06120		Copper chaperone PCu(A)C	1.98	0.03	
MPAO1_14990		NAD(P)-dependent alcohol dehydrogenase	2.22	0.01	
MPAO1_02740	*nirS*	Nitrite reductase	2.52	0.00	
MPAO1_25230		DUF748 domain-containing protein	1.85	0.02	
MPAO1_18000	*ccoP*	Cytochrome-c oxidase, cbb3-type subunit III	1.60	0.05	
MPAO1_28880	*adhP*	Alcohol dehydrogenase AdhP	2.52	0.00	
MPAO1_07010		Phosphoketolase	2.07	0.00	
MPAO1_00100		LysM peptidoglycan-binding domain-containing protein	1.44	0.03	
MPAO1_02290		TonB-dependent receptor	1.66	0.01	
MPAO1_27435		Amino acid ABC transporter substrate-binding protein	-3.09	0.03	
MPAO1_05385		DUF1302 domain-containing protein	-2.80	0.03	

MPAO1_17965	*acnA**	Aconitate hydratase	1.49	0.01	[48]
MPAO1_24155	*pilY1**	Type 4a pilus biogenesis protein PilY1	1.54	0.01	[49]
MPAO1_05375		Fatty acid--CoA ligase	-5.06	0.01	
MPAO1_04650		OmpW family protein	1.49	0.01	
MPAO1_00495	*tssH*	Type VI secretion system ATPase TssH	1.27	0.03	H1-T6SS [44]
MPAO1_14010		Non-ribosomal peptide synthetase (NRPS)	1.90	0.02	
MPAO1_26210	*azu*	Azurin	2.45	0	
MPAO1_13620		Xanthine dehydrogenase family protein molybdopterin-binding subunit	-4.33	0.01	
MPAO1_03800	*pchA*	Salicylate biosynthesis isochorismate synthase	-3.04	0.01	
MPAO1_06095		TonB-dependent copper receptor	1.74	0.00	
MPAO1_03775		Catalase	1.67	0.00	
MPAO1_02430	*clpG*	AAA family protein disaggregase ClpG	2.31	0.00	
MPAO1_26945		Poly(3-hydroxyalkanoate) granule-associated protein PhaF	1.22	0.03	
MPAO1_23990		Prepilin-type cleavage/methylation domain-containing protein	3.01	0.00	
MPAO1_02180		Response regulator	1.13	0.00	
MPAO1_05390		DUF1329 domain-containing protein	-2.62	0.00	
MPAO1_13900		NADP-dependent glyceraldehyde-3-phosphate dehydrogenase	-1.11	0.05	
MPAO1_13035		Multidrug efflux RND transporter periplasmic adaptor subunit MexE	-1.92	0.00	
MPAO1_25100		TonB-dependent hemoglobin/transferrin/lactoferrin family receptor	-1.17	0.02	
MPAO1_09260		Carbohydrate ABC transporter substrate-binding protein	-0.99	0.02	
MPAO1_16835		Porin	1.34	0.00	
MPAO1_09280		Porin	-1.54	0.00	
Planktonic only					
MPAO1_23930	*puiA***	TonB-dependent siderophore receptor	-6.91	0.00	
MPAO1_22860	*pctC*	Methyl-accepting chemotaxis protein PctC	-6.78	0.00	
MPAO1_07425	*argF*	Ornithine carbamoyltransferase	-5.51	0.01	
MPAO1_21260		Chain-length determining protein	-5.22	0.02	
MPAO1_15475		Siderophore-interacting protein	-5.09	0.02	
MPAO1_29055		Class I SAM-dependent methyltransferase	-5.08	0.03	
MPAO1_22680		Biliverdin-producing heme oxygenase	-5.02	0.03	
MPAO1_09305	*pgl*	6-phosphogluconolactonase	-5.01	0.03	